Summer 2019

Synthesis and Characterization of Gd-Doped InP/ZnS Quantum Dots for Use in Multimodal Imaging Probes

Molly Erin Duszynski
Missouri State University, Duszynski314@live.missouristate.edu

SYNTHESIS AND CHARACTERIZATION OF GD-DOPED INP/ZNS QUANTUM DOTS FOR USE IN MULTIMODAL IMAGING PROBES

A Master's Thesis

Presented to

The Graduate College of

Missouri State University

In Partial Fulfillment

Of the Requirements for the Degree

Master of Science, Chemistry

By

Molly Erin Duszynski

August 2019

SYNTHESIS AND CHARACTERIZATION OF GD-DOPED INP/ZNS QUANTUM DOTS FOR USE IN MULTIMODAL IMAGING PROBES

Chemistry

Missouri State University, August 2019

Master of Science

Molly E. Duszynski

ABSTRACT

Quantum dots (QDs), which are intensely fluorescent nanocrystals ranging 2-10 nanometers in diameter, have shown promise in fluorescence imaging. However, *in vivo* applications of QDs are limited due to the opaque surrounding of tissue and bones. In this study, InP/ZnS QDs were doped with a paramagnetic atom in an attempt to render them MRI-active. We have further bioconjugated these nanoprobes to develop highly specific MRI-active probes that can be used for detection of neurodegenerative diseases. These bioconjugated nanoprobes detect a mutated form of alpha-synuclein that forms oligomers that are a hallmark of Parkinson's disease and other alpha-synucleinopathies. Here, we have optimized the doping of QDs with MRI-active metals (*e.g.* Gadolinium) and characterized the MRI activity. The resulting nanocrystals were further studied to assess the success of the paramagnetic atom's incorporation into the crystal lattice and its performance as a probe for alpha-synucleinopathies such as Parkinson's disease.

KEYWORDS: quantum dots, magnetic resonance imaging, nanoparticles, bioconjugation, synthesis

SYNTHESIS AND CHARACTERIZATION OF GD-DOPED INP/ZNS QUANTUM DOTS FOR USE IN MULTIMODAL IMAGING PROBES

By

Molly E. Duszynski

A Master's Thesis
Submitted to the Graduate College
Of Missouri State University
In Partial Fulfillment of the Requirements
For the Degree of Master of Science, Chemistry

August 2019

Approved:

Katye M. Fichter, Ph.D., Thesis Committee Chair

Gary Meints, Ph.D., Committee Member

Fei Wang, Ph.D., Committee Member

Kartik Ghosh, Ph.D., Committee Member

Julie Masterson, Ph.D., Dean of the Graduate College

ACKNOWLEDGEMENTS

I would like to thank Dr. Katye Fichter for allowing me to work in her lab, perhaps against her better judgment. Even beyond that, I have to thank her for getting me through the last year of my master's degree from 600 miles away without getting paid. She has had to put up with a lot over the past couple years. Thank you for the patience and believing that, somehow, I could do this without your direct supervision. I would also like to thank Greg Illy and Teddy Illy for the phone calls, pictures, motivation, and being my number one supporter even long distance. Furthermore, I would like to thank Dr. Gary Meints, Dr. Gautam Bhattacharyya, Dr. Fei Wang, and Dr. Kartik Ghosh. Thank you to Rishi Patel at Jordan Valley Innovation Center (JVIC) for help with microscopy, and Dr. Rich Biagioni and Jabez Campell for assistance with ICP-MS. Lastly, I would like to thank my friends inside and outside of the department who have seen me at my best and my worst and still answered the phone the next day.

A portion of this work was performed at the National High Magnetic Field Laboratory, which is supported by the National Science Foundation Cooperative Agreement No. DMR-1644779 and the State of Florida. Additionally this material is based upon work supported by the National Science Foundation under Grant No. 1828069.

I dedicate this thesis to Sonia M. Giles.

TABLE OF CONTENTS

LIST OF FIGURES

LIST OF FIGURES CONTINUED

CHAPTER 1: INTRODUCTION

1.1 Quantum Dots

Quantum dots (QDs) are highly fluorescent semiconductor nanocrystals that have size-dependent optical properties. QDs are typically about 2-10 nm in diameter and composed of anywhere from hundreds to thousands of atoms[1,2,3,4]. QDs composed of group II-VI elements (e.g., CdS or CdSe) had been popular for use in biomedical research; however, studies have shown that Cd-based QDs can be degraded in a biological environment, leading to release of cytotoxic Cd^{2+} ions[4]. For this reason, researchers investigated alternative QDs with a more biologically compatible core, composed of group III-V elements (*i.e.* InP)[3]. Compared to conventional organic dyes, QDs are resistant to photobleaching, giving them the potential to be used long-term[1]. Additionally, they can be easily biofunctionalized for applications in biomedical research, diagnostics, and therapeutics[4,5].

QDs exhibit size-dependent optical properties, such as absorbance and photoluminescence, that fall in between a bulk semiconductor and discrete molecule[6,7]. The physical radius of a QD is smaller than the material's Bohr radius, which is described as the separation between an excited electron in the conduction band and the hole it leaves in the valence band[8]. The confinement of electrons into a quantum box causes a conversion from continuous to discrete energy levels. For QDs with a smaller size, the difference in energy between valence and conduction bands is much larger, requiring more energy for excitation, but also releasing more energy as the electron returns to the ground state. As the size of the QD increases, the band gap decreases resulting in a red-shift (Figure 1)[9]. Because of this, the relative

size distribution in QDs can be observed as the full-width half maximum in a fluorescence emission spectrum.

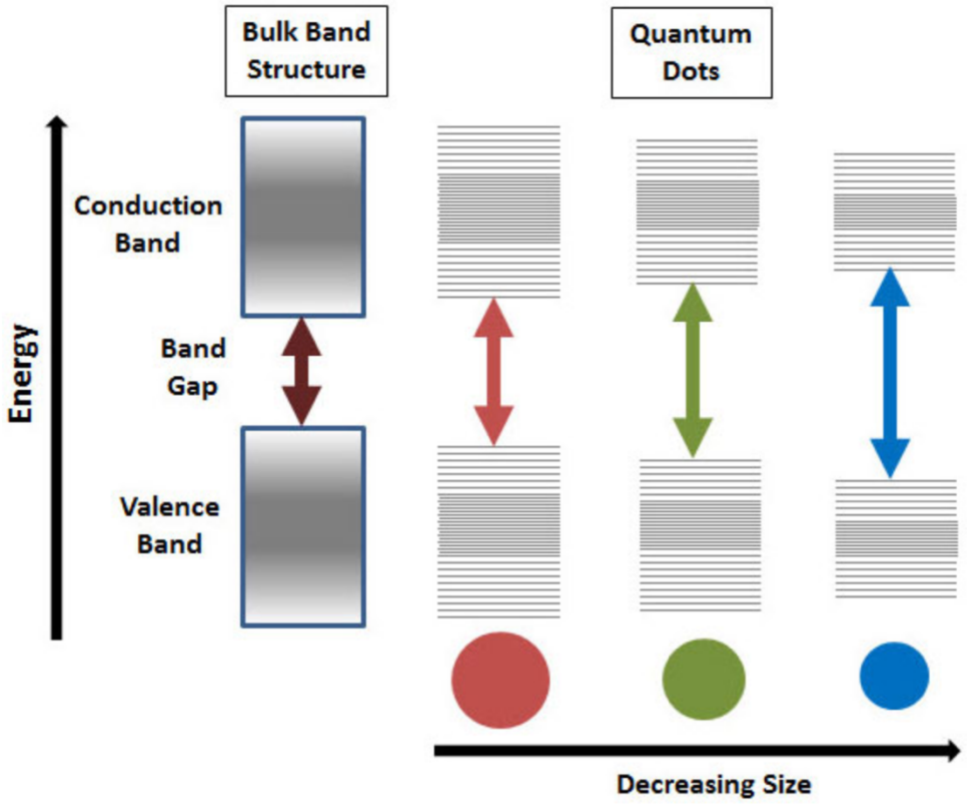

Figure 1: Band gap energy and emission of QDs[10]. The band gap of a respective QD has an inverse relationship with size, due to quantum confinement. The larger the size, the smaller the band gap and energy.

During fluorescence, an excited electron can proceed through two different relaxation processes: radiative and non-radiative decay (Figure 2). In radiative decay, light is emitted as a result of relaxation. In the case of non-radiative decay, however, energy is released instead as heat, and electrons move from a high energy level to a meta-stable level[6,7]. Defects on the QD, also known as surface traps, act as sites for nonradiative decay. Some of the excited electrons can decay to these surface traps located mid band gap. They then nonradiatively recombine with the holes located in the valence band, reducing photoluminescence quantum yield[8]. Placing an

inorganic shell with a large bandgap over the QD core (sometimes referred to as "shelling") can help to passivate these defects and improve fluorescence as well as photostability[1].

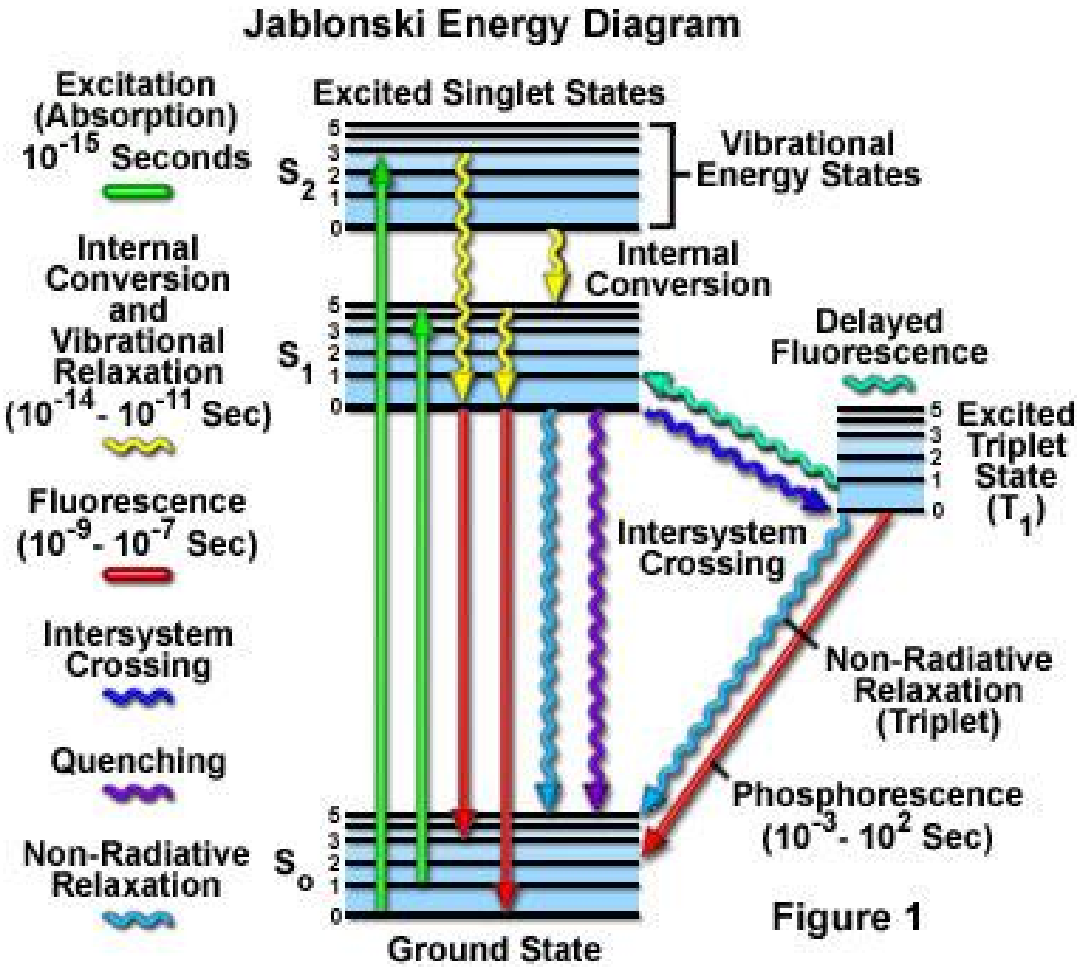

Figure 2: Jablonski energy diagram[11]. The Jablonski diagram shows different paths of relaxation an electron can proceed through after reaching an excited state.

InP nanocrystals are prone to surface oxidation and photodegradation, and ultimately, poor fluorescence. To mitigate this, the InP core is often shelled as mentioned above, promoting stability and increasing photoluminescence[5]. In a Type I (*e.g.* InP/ZnS) core/shell composition, the conduction band of the shell is at a higher energy than the core, while the valence band is at a lower energy than that of the core, effectively confining both the electrons and their holes to the core (Figure 3)[1,12]. This has been shown to increase photoluminescence quantum yield by

reducing nonradiative recombination[12]. In deciding on a core and shell, the materials must have analogous crystal structure with lattice mismatch below a threshold to feasibly allow for shell growth (~12%)[13]. ZnS in advantageous as a coating material for InP QD cores since the lattice mismatch is only 7.6% and it is chemically stable and nontoxic[12,13].

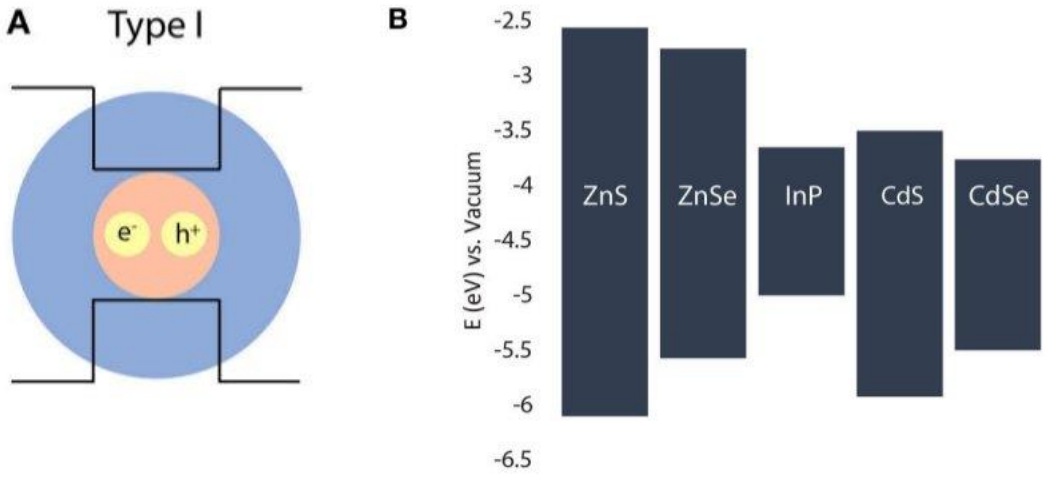

Figure 3: Core/Shell bandgap distribution[12]. (a) In a Type I core/shell structure, the band gap of the shell material, pictured on either side of the core, confines both the electron and its hole to the core. (b) Positions of both valence and conduction bands for various semiconductor materials. ZnS's band gap easily confines that of InP.

1.2 Synthesis

There are several methods for synthesizing QDs, but most relevant method for this work is hot-injection, where precursors are injected into the heated reaction mixture during synthesis[14]. Before the reaction is started, precursors for indium and zinc are added to a coordinating solvent, the temperature is increased, and an inert atmosphere is introduced. Addition of the phosphorous precursor initiates the crystallization of the QDs, which can be broken up into three stages: precursor conversion, nucleation, and growth. All three steps occur in rapid succession, making the study of the kinetics of crystallization difficult[16].

In the first step, called precursor conversion, phosphine and indium species present in the reaction mixture interact to form InP monomers (Figure 4). One of the prevailing theories

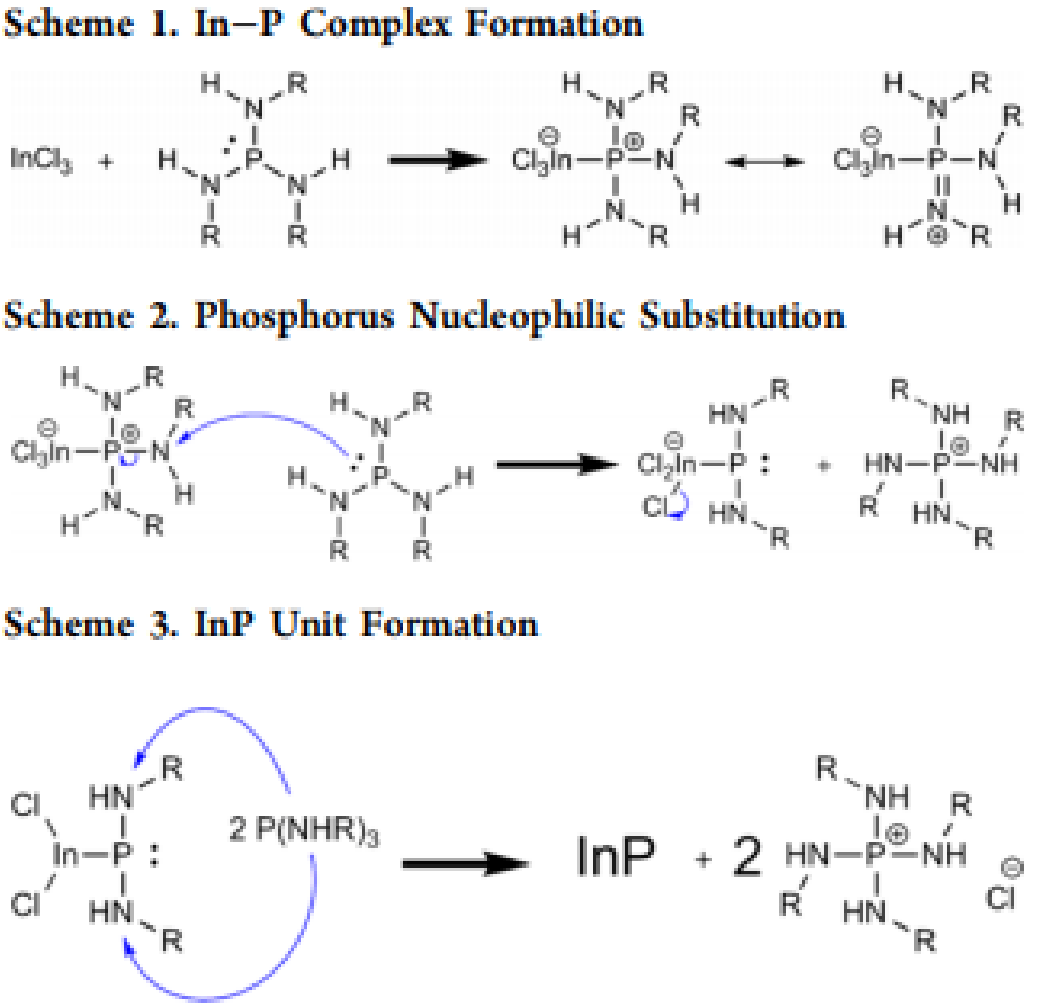

Figure 4[17]: InP formation. (Scheme 1) $InCl_3$ forms an adduct with the aminophosphine with a delocalized positive charge, allowing for (Scheme 2) a nucleophilic attack by a second aminophosphine group leading to an InP intermediate and phosphonium salt. (Scheme 3) Two more equivalents of the aminophosphine further reduce the phosphorous of the intermediate to an oxidation state of -III, forming InP.

postulates that formation of InP from $InCl_3$ and tris(dimethylamino)phosphine (TDMAP) is dependent on the type of coordinating solvent used[17]. In order for the reaction to take place, the coordinating solvent must have a primary amine, such as oleylamine[17]. This allows TDMAP to

undergo transamination, a nucleophilic attack from the phosphorous center of one TDMAP on the amino group of another. The resulting fully transaminated product then proceeds as a reactant. In order for this reaction to proceed, there must be ~4 times as much TDMAP as there is $InCl_3$; 3 equivalents of transaminated aminophosphine reduce a fourth in order to form the InP monomer through oxidation and reduction[17].

Following the precursor conversion to InP, nucleation and growth occur. Classically, nucleation and growth are described using LaMer's model that separates nucleation and growth into two steps, which is essential for synthesizing monodisperse nanocrystals (NCs). In this model, a rapid burst of nucleation occurs directly followed by the growth stage[16]. Here, this is achieved using hot-injection of a phosphorous precursor to trigger monomer formation, followed by a burst of nucleation. As nuclei form, the monomer concentration decreases, and NCs move into the growth stage[18]. During growth, NC size can increase when smaller NCs dissolve, a process called Ostwald ripening[16]. This effect can lead to a larger size distribution of NCs.

Once core growth is terminated, shelling can be initiated. Previous work has suggested that oleylamine ligands and the zinc precursor species passivate the surface of the InP cores, providing a Zn-rich surface for growing ZnS shells (Figure 5)[18]. Shell formation is initiated by addition of a sulfur precursor (*e.g.* dodecanethiol). Additional shelling is facilitated by the addition of more zinc precursor, which improve photostability and quantum yield[20]. During shelling, dodecanethiol binds with the ZnS on the surface, becoming the surface capping ligand for the final core/shell QD product[18].

For QDs to be biologically relevant, they must be water-soluble, which requires exchanging the existing surface ligands for water-soluble ligands. 11-mercaptaundecanoic acid is often used as a water-soluble surface ligand due to its facile exchange and binding energy[21]. The

$Zn\text{-}S_{thiolate}$ binding energy (194.7 kJ/mol) is higher in comparison to both a $S\text{-}S_{thiolate}$ and $Zn\text{-}S_{thiol}$ with binding energies of 105.1 kJ/mol and 31.8 kJ/mol, respectively[22]. Tetramethylammonium hydroxide (TMAH) is used as a base to deprotonate the thiol of MUA. The deprotonated MUA forms ion pairs with tetramethylammonium cations, allowing it to be transferred into the chloroform solvent. This gives rise to the bond between the thiolate and ZnS surface, allowing the QDs to ultimately be transferred to the aqueous phase[21].

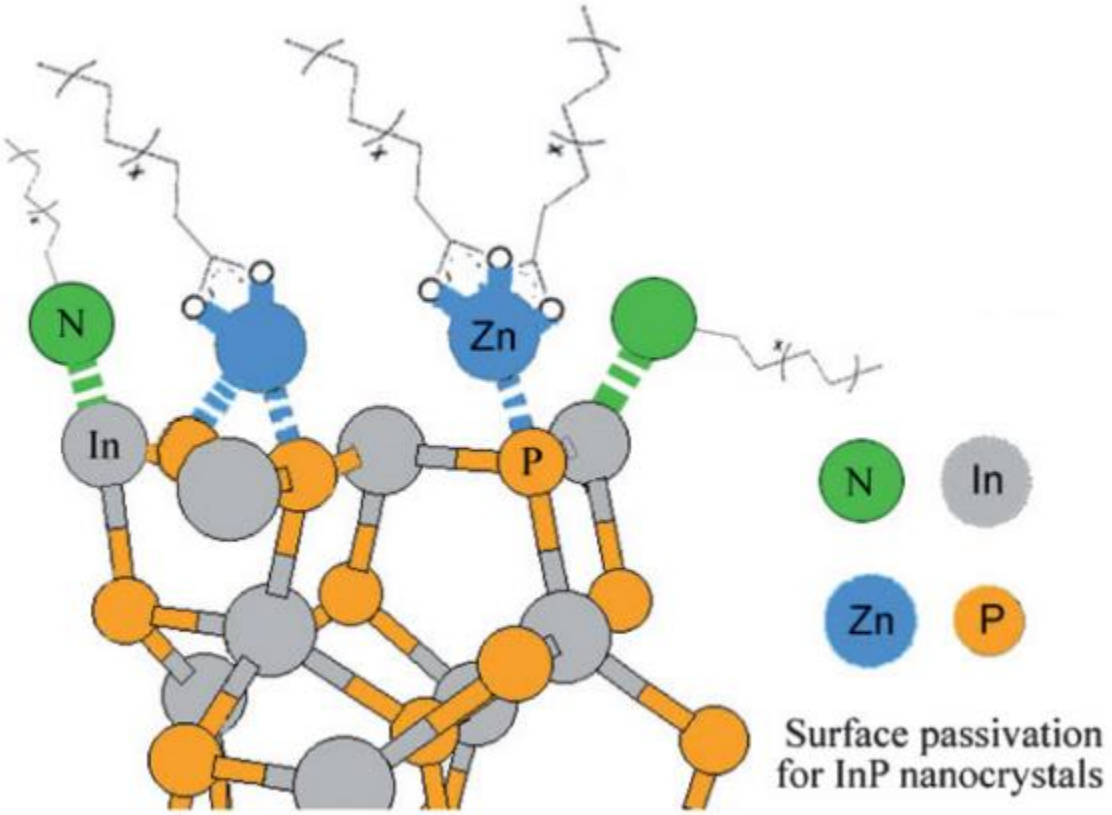

Figure 5: Surface passivation of InP cores[19]. Leading up to shell formation, oleylamine ligands and zinc stearate passivate the surface of the cores.

1.3 QD Doping

One way to impart optical, magnetic, electrical, and electronic properties to QDs is by doping the structure with an impurity. Impurity states introduced by a dopant allow for high

quantum yield emissions and have been documented to cause a red-shift in emission, possibly due to dopant d-d levels or interaction of the dopant d level with the core material[23]. Examples have included Cu and Mn, with the latter showing a marked improvement in quantum yield[23,24]. Doping of QDs can be performed either extrinsically or intrinsically. Extrinsic doping is characterized by two types: charge injection methods or the use of certain surface ligands to induce further functionality of QDs[24]. Intrinsic doping involves doping the core of the QD by nucleation, growth doping, or ion diffusion[24,25]. In the ion diffusion method, the dopant precursor is incorporated into the reaction mixture prior to nucleation or growth. Ion diffusion can separately be broken down into cation exchange for diffusion doping[23]. In this work, doping is used to introduce Gd^{3+} as a core dopant using intrinsic methods.

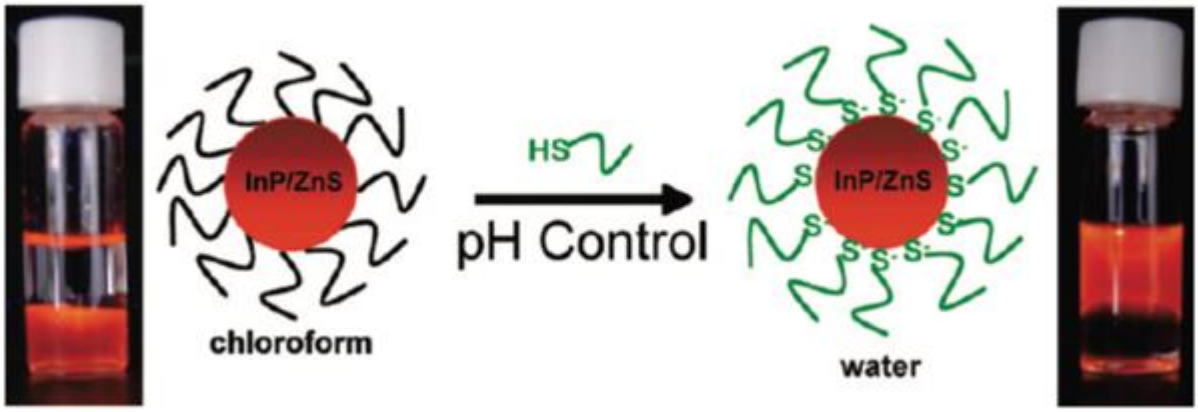

Figure 6: QD phase transfer[21]. InP/ZnS QDs shown on the left are in organic solvent (bottom phase) with dodecanethiol surface ligands. On the right, QDs transfer to the upper aqueous phase with MUA surface ligands.

1.4 Magnetic Properties

The desired properties of the QD determines the choice of dopant. Magnetic functionality has been of recent interest for its potential in multimodal imaging[26,27]. By imparting magnetic

properties to QDs, they could be used to provide contrast in magnetic resonance imaging (MRI), a method critical for clinical diagnostics in disease and injury[26]. Manganese (Mn^{2+}) and Gadolinium (Gd^{3+}) are the most common paramagnetic ions used as contrast agents for MRI. For this reason, they are being investigated for incorporation into QD structures[26]. By doping QDs with a paramagnetic ion, relaxivity per QD is larger than it would be per ion due to the ability for each QD to host many paramagnetic ions[1,27]. This characteristic is useful for magnetic probes with a molecular target.

The magnetic properties of a paramagnetic ion are of particular interest for use in nuclear magnetic resonance (NMR). In a paramagnetic ion, there is a minimum of one unpaired electron, behaving as a tiny magnet. In the presence of a strong external magnetic field (B_0), nuclear spins can adopt either a parallel or antiparallel orientation in relation to the external field (Figure 7); the nuclear spin represents the total angular momentum of a nucleus and is associated with a magnetic moment[28,29]. Of the two orientations, parallel alignment occurs as the lower energy state, making it the preferred alignment, though the energy difference between the states is relatively small[29]. This difference, however, results in a net magnetization vector (Mz) aligned to the magnet. Individual nuclei do not line up with the field but wobble, or precess, around the direction of the magnetic field at a frequency described by the Larmor equation[28].

In order to gain information regarding the nuclear spin, the direction of the net magnetization factor (Mz) must be changed to give a measurable signal. This is done by exciting the spins using radiofrequency (RF) pulses[28,29]. The energy from the RF pulse is absorbed by protons, thus allowing them to go from a parallel state to antiparallel. The spins then precess in phase, and Mz align 90° into the transverse plane. When the RF transmitter is off, nuclei return to their ground state, magnetization in the transverse plane decreases, and the induced signal

decreases, referred to as free induction decay (FID). The time it takes for the signal to return to equilibrium is the relaxation time[28].

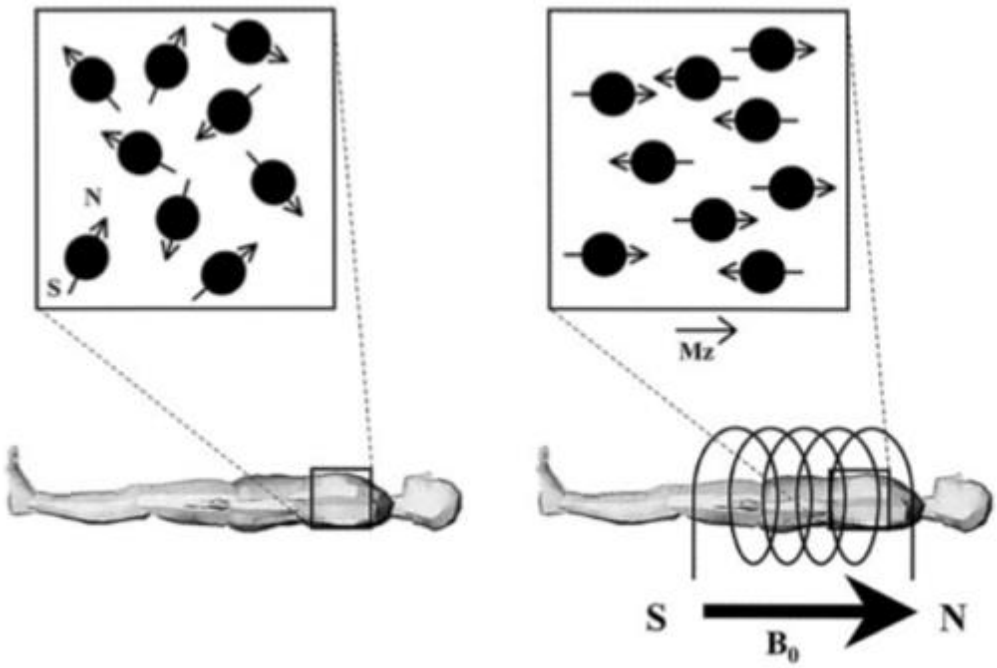

Figure 7: Effect of magnetic field on nuclear spin[28]. Without a magnetic field, magnetic moments have random distribution. With the application of a strong external magnetic field, spins align in an antiparallel or parallel fashion. The net magnetization vector (Mz) runs parallel with B_0.

Relaxation can be described with two different constants: T_1 (longitudinal) and T_2 (transverse). T_1 is characterized by realignment with B_0 toward a spin's thermal equilibrium value. T_2, however, is characterized by the decay of coherence: after an RF pulse, spins are in phase, but as time passes, the signal decreases as spins begin to dephase from inhomogeneities or spin-spin interaction. The T_2 time is always shorter than T_1. Signals from these measurements can be converted using Fourier transform to corresponding intensity, which is pixel mapped into shades of gray in an image (Figure 8)[28,29].

Generating data for T_1 and T_2 times require different methods of data collection. Repetition time (TR) refers to the length of time between RF pulses applied to a sample. Time to Echo (TE) measures the time between the RF pulse and the echo signal. In general for T_1, short TE and TR times are used, while T_2 images are produced with longer TE and TR times[28,29].

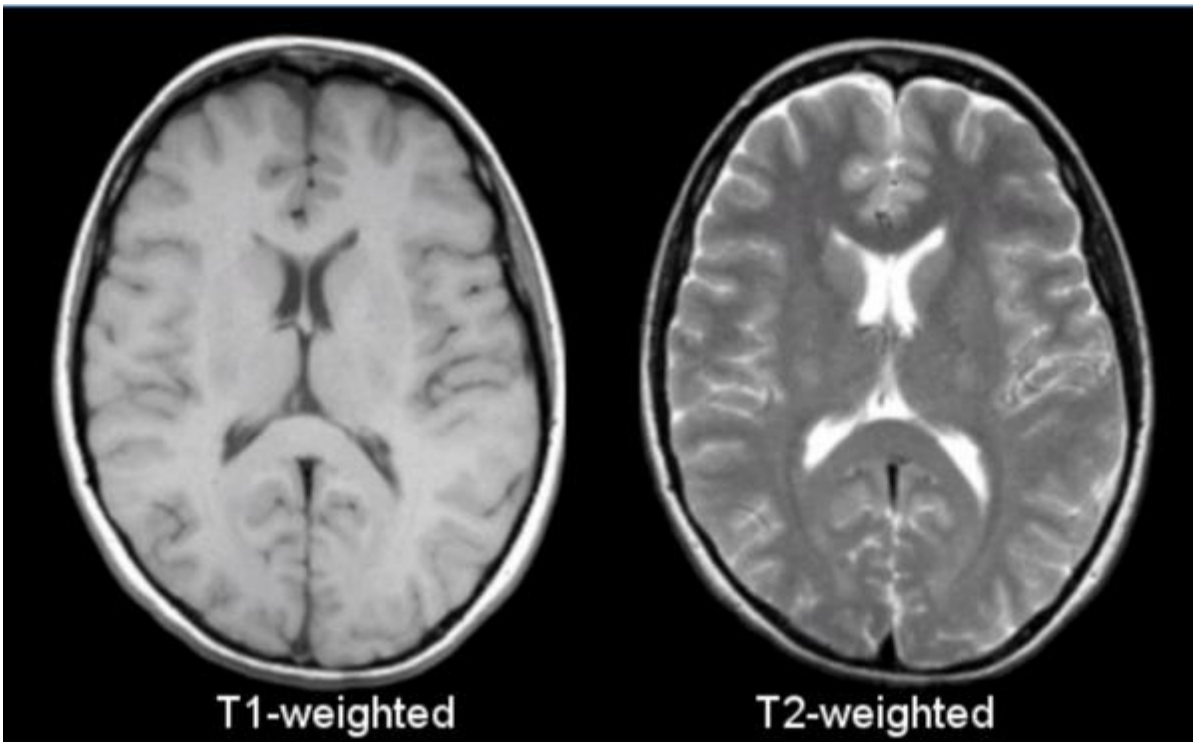

Figure 8: T_1 vs T_2 weighted images[30]. Notable differences between T_1 and T_2 images in the brain are shown here. T_1-weighted images show the cerebral spinal fluid (CSF) dark. In a T_2 weighted image, however, CSF is bright with higher pixel intensity.

1.5 Biomedical Application

Parkinson's disease (PD) is a neuromuscular disease characterized by the degeneration of dopaminergic neurons in the *substantia nigra* region of the brain. Usually by the time a patient starts presenting with motor impairment, >50% of dopaminergic neurons and up to 80% of synaptic activity are lost in this region, taking place over years preceding diagnosis[31]. The disease is often able to progress quite far before therapeutic intervention due to difficulties in

diagnosing PD and problems with patients self-reporting symptoms. Currently, to diagnose a patient with PD, a doctor must take a patient history and consider the symptoms reported by the patient. Because this decision is largely based on patient self-reporting, there is potential for inaccuracies. No definitive test exists at this time to diagnose a living patient, since PD can only be confirmed on autopsy with microscopic observation of the affected neurons[31,32].

One possible target for developing a diagnosis method lies with a defining trait of PD. The hallmark of PD is the presence of Lewy bodies, structures in the cytoplasm of neurons that contain aggregates of misfolded protein alpha-synuclein[32,33]. Alpha-synuclein is a 140-residue protein that has been shown to aggregate, or oligomerize, in disease states, interfering with neuron signaling[33]. Previous work in our lab has established a method by which QDs can be bioconjugated to a peptide that binds to toxic alpha-synuclein oligomers. Coupling this peptide-binding detection method with Gd-doped QDs could allow for the development of an MRI-based method to detect and observe the progression of PD.

1.6 Assessing QD Toxicity

Before Gd-doped QDs can be used in biological applications, a toxicity assay should be performed to determine the effects of the presence of Gd in the Gd:InP/ZnS QDs. One way to determine toxicity of nanoparticles or drugs on cells is through a colorimetric assay based on 3-[4,5-dimethylthizol-2-yl]-2,5 biphenyl tetrazolium bromide (MTT)[34]. Since most viable cells have constant mitochondrial activity, cellular viability can be measured by the activity of succinate dehydrogenase, a crucial mitochondrial enzyme. When MTT is in the presence of active succinate dehydrogenase, it is reduced to MTT-formazan, which is a purple crystal. Once MTT-formazan has formed inside the cells, the cells can be lysed using a detergent. The crystals

then are solubilized, and the formazan quantified via absorbance at 570 nm. An increase or decrease in formazan concentration depicts increased or decreased mitochondrial activity (*i.e.* cellular viability)[35]. In order to generate a standard curve to quantitate viability, cells are plated at concentrations appropriate to the cell line and are dependent upon rate of proliferation and mitochondrial activity; here, the cell were plated at 500 – 2,750 cells per well. Plating at too high of a cell density can lead to a plateau in cell growth from contact inhibition, exhaustion of cell medium, and exceeding maximal OD value for measurement. In order to assess the effect of a QD sample on cell viability, a range of QD concentrations replicating that usually used for cell treatment is selected. After plating cells at a concentration that falls in the range of the standard curve, cells are allowed to proliferate for 24 hours before being treated in triplicate with QDs for an additional 24 hours. After this, each well is treated as previously described with MTT and subsequently a detergent. The measured absorbance of the lysed QD-treated cells is compared against the lysed control cells (not treated with QDs) to determine the percent cell viability[34,35].

In InP/ZnS QDs, known for their decreased toxicity, were doped with Gd. The amount of Gd used in the initial reaction for core nucleation growth was varied to determine how much Gd was incorporated into the nanocrystal, and how this affected the relaxation time of the QD. Additionally, one QD synthesis was performed to attempt to incorporate Gd into the shell of the QD to see if the closer proximity of Gd to the surface (and thus nearby water molecules) would increase relaxation in comparison to core doping. Post-synthesis characterization by UV-Vis spectroscopy and fluorimetry was used to determine the optical properties and size distribution of each QD sample. Scanning Transmission Electron Microscopy (STEM) was performed to determine whether Gd had an effect on size or size distribution. To determine the success of doping, Inductively Coupled Plasma (ICP) spectroscopy was used to obtain molar ratios of

elements present in QDs and assess the amount of Gd incorporated into the QD. Further studies were done investigating the relaxation potential of samples and cell viability to determine the effect these QDs would have at similar concentrations to those seen in normal cell targeting studies. From this work, properties such as monodispersity, NMR relaxation potential, and cytotoxicity determine whether Gd:InP/ZnS QDs are indeed feasible as a diagnostic tool.

CHAPTER 2: EXPERIMENTAL

2.1 Reagents

All chemicals were purchased from Millipore Sigma (St. Louis, MO) except for the following: $InCl_3$ 99.995% (193190100, Acros Organics), $GdCl_3$ anhydrous (93-6416, Strem), 200 proof ethyl alcohol (200-CSPTP, Ultrapure), Sodium phosphate dibasic anhydrous (BP332-500, FisherBiotech), 1-dodecanethiol (117625000, Acros Organics), methanol (A434-20, Fisher Chemical), and sodium dodecyl sulfate (SDS) (61-1043, BioPhore).

2.2 Core/Shell QD Synthesis

Prior to synthesis, all glassware was cleaned in a base bath of 8% KOH in 3:1 EtOH:H_2O. The synthesis method used here was an adaptation from previous work[36]. 0.903 mmol $InCl_3$ and 1.83 mmol Zn stearate was added to a 100 mL round bottom flask (RBF) containing 30 mL oleylamine and a stir bar. The RBF was placed in a heating mantle over a stir plate and connected to a proportional-integral-derivative (PID) temperature controller with temperature probe. The mixture was stirred, and the RBF was placed under a vacuum for 1 hour, then the temperature was increased to 120°C and the RBF was evacuated further for 20 minutes. The RBF was then filled with argon gas and the temperature raised to 230°C and allowed to stabilize for 15 minutes. To initiate core nucleation and growth, 1 mL tris(dimethylamino)phosphine was quickly injected. After 9.5 minutes, the reaction was removed from heat and allowed to cool to 200°C to terminate core formation. The temperature was then increased to 240°C and 6 mL dodecanethiol was slowly added to the reaction mixture to begin passivation of the QD cores with a ZnS shell. After 3 hours, an additional 1.85 mmol Zn stearate (dispersed in 10 mL

oleylamine) was slowly injected. The reaction was allowed to proceed for 3 more hours, then cooled to 60°C, and 10 mL of hexanes added. The resulting solution was then transferred to a 50 mL centrifuge tube and centrifuged at 3,000 x g for 10 minutes. To wash the QDs and remove excess organic ligands, the supernatant was separated into two 50 mL centrifuge tubes, 70% methanol: 30% chloroform was added to bring the total solution to 50 mL, and the solution was centrifuged again at 3,000 x g for 10 minutes. The resulting pellet was then redissolved in 10 mL chloroform and the washing step repeated two more times. QD samples were stored at -20°C. For core doped QDs, in the initial reaction vessel, either 0.224 mmol, 0.336 mmol, or 0.336 mmol $GdCl_3$ was added to the original $InCl_3$, Zn stearate, and oleylamine mixture before the reaction started. In the case of the shell doped sample, 0.224 mmol $GdCl_3$ was suspended in 6 mL dodecanethiol and slowly injected during shelling.

2.3 UV-Vis Spectroscopy

For UV-Vis spectroscopy, stock solutions of all samples were diluted 10-fold, with the exception of the shell-doped QDs, which were diluted 2-fold to preserve the signal-to-noise ratio in the spectra. QD samples were placed in a 60 μL cuvette (path length of 0.3 cm) and scanned at a rate of 51 nm/min from 750 nm to 300 nm. For analysis of the data (particle size and concentration), calculations were used from literature on InP/ZnS QD kinetics[37]. To determine the stock concentration, the maximum wavelength and absorbance of the shoulder peak was used. To first determine particle size the following equation was used:

$$particle\ size = 0.1456e^{(0.0052 \times \lambda)}$$

where λ is the maximum wavelength of the shoulder peak. The extinction coefficient was then calculated using:

$$\frac{\varepsilon}{10^6} = 0.0092(particle\ size)^{3.959}$$

From here, Beer's law was used to calculate the concentration of the solution:

$$A = \varepsilon L c$$

where L is the path length of the cuvette, A is the absorbance at the maximum wavelength, c is concentration in units, and ε is the previously calculated extinction coefficient.

2.4 Fluorescence Spectroscopy

To perform fluorescence spectroscopy, all samples were diluted to 1 μM and the cuvette rinsed with chloroform between each sample. Emission spectra were collected using an excitation wavelength of 250 nm and data collected from 400-800 nm, covering the visible range. All slit widths were set to 5 nm and the step size and integration set to 1 nm and 1 sec respectively to reduce the signal to noise ratio and make it easier to elucidate all spectral characteristics.

2.5 QD Water Solubilization

Prior to ligand exchange, the QDs were washed again by adding 15 mL degassed ethanol to 5 mL QDs (a ratio of 3:1) and centrifuging at 3,000 x g for 5 minutes. The pellet was

resuspended in degassed chloroform, and the wash step repeated once more. 12.5 mmol tetramethylammonium hydroxide (TMAH) was dissolved in 25 mL of DI water to make a 0.5 M solution. 12.5 mmol of 11-mercaptoundecanoic acid (MUA) was then dissolved in this TMAH solution to make a final solution consisting of 0.5 M TMAH and 0.5 M MUA. Equal volumes of QDs in chloroform and 0.5 M TMAH/MUA were combined and stirred vigorously to create an emulsion for 12-24 hours.

The solution was then centrifuged at 3,000 x g for 5 minutes to separate the organic and aqueous layers. The aqueous layer (top) was collected and the organic layer (bottom) was discarded, and the aqueous layer was further centrifuged at 17,000 x g to ensure full separation from organics. To purify the QDs, they were dialyzed for 4 days in 300 kD MWCO dialysis units against 4L 0.01 M phosphate buffer (pH 11.5) with frequent replacement of the buffer. The resulting samples were then filtered through a 0.22-micron filter in a 1 mL syringe to remove aggregates. Water soluble QDs were stored at 4°C.

2.6 Scanning Transmission Electron Microscopy (STEM)

A 10 μL volume of QD solution was pipetted onto ultrathin carbon on lacey carbon coated copper TEM grids (Tedpella PN: 01824). After 2 minutes of settling time, the excess solution was wicked away and the remaining volume was left to evaporate in a vacuum desiccator. The TEM grids were then imaged with a scanning transmission electron microscopy (STEM) detector on a thermal field emission scanning electron microscope (FESEM). Imaging was done with a KE Developments STEM detector in bright field mode on a JEOL 7600F FESEM at 30 kV acceleration voltage.

2.7 ICP/MS

For QD sample preparation, approximately1 mg of each sample was dissolved in 1 mL of nitric acid and sonicated, and then an internal standard stock (ISS) was added to a final concentration of 5 μL/mL. Each sample was then diluted to 10 mL with DDI water and nitric acid to a final concentration of 20% nitric acid. To create standard curves for each element, concentrations of 5,000, 10,000, and 50,000 ppb were used for P, S, Zn, and In; for Gd, 500, 1,000, and 5,000 ppb standards were used. In the method used, P-31, S-34, and Zn-66 were monitored with Sc-45 as the internal standard (IS), In-255 with Cd-111 as the IS, and Gd-157 with La-139 as the IS. Each sample was run with a 60 sec uptake, 40 sec sample stabilization, 10 sec water rinse, 10 sec acid rinse, and 20 sec probe rinse through 1.05 L/min nebulizer argon flow and a 1550 W plasma. The integration for all masses was 0.50 s.

2.8 Cell Culture

All cell culture reagents were purchased from HyClone (Logan, UT) except the following: Fetal bovine serum (35-010-CV, Gibco), 0.25% Trypsin-EDTA (25200-056, Gibco), Sodium Pyruvate (11360-070, Gibco), FluoroBrite™ DMEM (A18967-01, Gibco), and 96 well plates (353072, Falcon). N2a (mouse neuroblastoma) cells were a kind gift provided by Dr. Tania Q Vu at Oregon Health and Science University.

In order to sustain the cell line, N2a cells were grown and split once every 2-3 days to maintain a suitable environment for healthy cells. When cells reached about 80% confluency, they were passaged using sterile technique in a biosafety cabinet. The media was aspirated from the cells, phosphate buffered saline (PBS) was added to wash away any excess media and aspirated away, and then trypsin added and the flask returned to the incubator for 4 minutes to

allow cells to detach from the surface of the flask. After this time, 3 mL DMEM was added and then mixture removed and placed in a 15 mL falcon tube. Here the mixture was then pipetted up and down to deaggregate cells before adding 0.5 mL of cells a new flask containing 5 mL of DMEM. Cells were returned to the incubator to incubate at 37°C and 5% CO_2.

2.9 MTT Cell Viability Assay

To generate a standard curve, N2a cells were plated into 96 well plates at 2,750, 2,500, 2,250, 2,000, 1,750, 1,500, 1,250, 1,000, 750, 500, and 250 cells/well in triplicate. For each QD treatment, 1,500 cells/well were plated in triplicate. The plate was incubated at 37°C and 5% CO_2 for 24 hours. To assess the toxicity of the QDs on N2a cells, 6 concentrations ranging from 250 pM - 500 nM of QDs were diluted with PBS. After the cells had incubated for 24 hours, a control of PBS and all 6 QD dilutions were applied in triplicate and the plates placed back in the incubator for another 24 hour period. Media was then replaced with 50 μL FluoroBrite™ DMEM media and 50 μL 0.5 mg/mL 3-(4,5-dimethylthiazol-2-yl)-2,5-diphenyltetrazolium bromide (MTT) in PBS and the cells were incubated for 3 hours to allow for formazan crystal formation. To lyse cells and solubilize the crystals, an additional 150 μL 10% SDS solution was added to each well and the cells were allowed to incubate for 30 minutes. The absorbance of each solution in the wells was then measured at 570 nm.

2.10 Magnetic Resonance Image Acquisition

MRI data were acquired on a 21.1 T (900 MHz) magnet at the National High Magnetic Field Laboratory (NHMFL) in Tallahassee, Fl. MRI scans were carried out on an ultra-wide bore

21.1 T (900 MHz) vertical magnet built at the NHMFL. The magnet was equipped with a Bruker Avance III console and data acquisition was performed with ParaVision 6.0.1 acquisition and processing (BioSpenCorp, Billerca, MA) software together with a 64 mm inner diameter high performance gradient (Resonance Research Inc, MA) capable of producing 0.6 T/m peak gradient strength. Different configurations and dilutions of the QDs were placed in 5-mm NMR tubes and 8 tubes at a time were imaged using a 33 mm home-built radio frequency (RF) coil. A Gd contrast agent gadodiamide (Omniscan™) and water were added as controls. All measurements were acquired with 2D axial orientation with a 150 x150 μm in-plane resolution and 1.5 mm slice thickness. For T_1 measurements, a turbo spin echo (SE) sequence was used. The echo time (TE) was 20 ms and incremented repetition times (TR) between 0.034-1.2s. T_2 relaxation were acquired with a multi slice multi echo (MSME) sequence using TR = 5,000 ms and incremented echo time (4.5 – 90ms). Regions of interest were placed within each tube and signal intensity data collected. Data were then fitted to an exponential rise to maximum (T_1) and exponential decay (T_2) functions using Matlab.

CHAPTER 3: RESULTS AND CONCLUSIONS

3.1 QD Synthesis

For the synthesis of all QD samples, hot injection synthesis was used. This method starts a burst of nucleation that then proceeds to the growth stage by rapidly injecting cooler precursors into the hot reaction mixture. In order to exclude any atmospheric water that may contribute to surface defects in the QDs, as well as affecting the hygroscopic precursor salts, the reaction must take place under an inert atmosphere. To achieve this, a vacuum was attached to the reaction set up and used to evacuate the system before subsequently flooding it with argon gas. A bubbler was added between the reaction set up and the vacuum as well as at the top exit vent for the inert gas. Five different samples were synthesized for this work using varying amounts of $GdCl_3$, named based off the mmol of Gd used in the reaction: non-doped InP/ZnS, Gd:InP/ZnS (0.224 mmol), Gd:InP/ZnS (0.336 mmol), Gd:InP/ZnS (0.448 mmol), and shell-doped Gd:InP/ZnS (0.224 mmol) QDs.

In order to ensure the synthesis proceeded as expected, several defining steps in the reaction were studied (Figure 9). Firstly, as TDMAP was injected, the success of core formation was assessed on the color change that occured. The reaction mixture started as a pale yellow-white color, but post-injection, began to darken, ultimately becoming a dark brown. Next, as dodecanethiol was added to begin shell passivation, successful shelling was assessed via UV radiation on the reaction mixture. If fluorescence is observed, the shelling process is likely proceeding, since InP cores are not inherently fluorescent. With every individual synthesis, samples appeared various shades of dark red under ambient light; however, when irradiated with UV light, the emitted fluorescent colors were more easily differentiated (Figure 10).

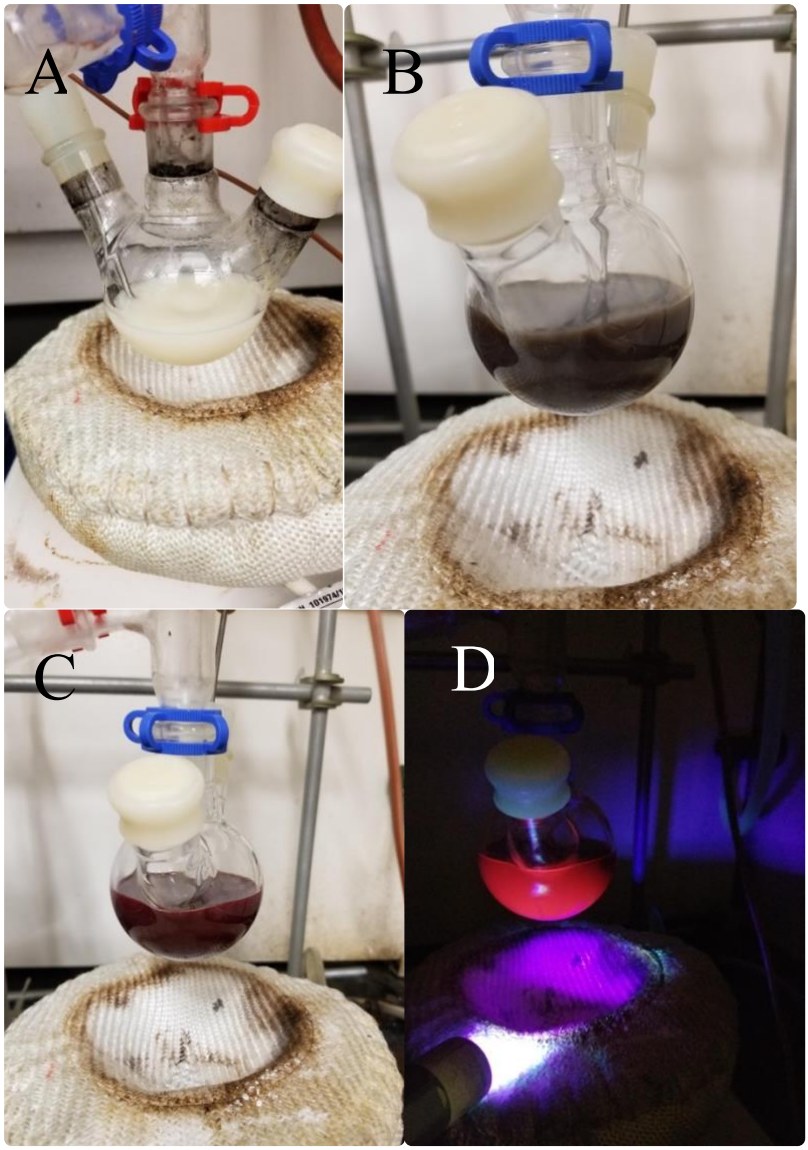

Figure 9: Appearance of QD synthesis under ambient light or UV light during core synthesis and shelling. A: Photo of QD synthesis under ambient light before injection of TDMAP. B: Photo of reaction mixture under ambient light after TDMAP injection and core formation. C: The reaction mixture following dodecanethiol injection as the mixture appears redder in ambient light. D: The final product of QDs with UV light to show fluorescence and a successful synthesis.

Post-synthesis, samples were cleaned by adding hexanes to the mixture and centrifuging. As the QDs are soluble in hexanes, this step was meant to remove oleylamine and any excess precursor chemicals. It was noticed that for samples Gd:InP/ZnS (0.336 mmol), Gd:InP/ZnS (0.448 mmol), and shell-doped Gd:InP/ZnS (0.224 mmol) QDs that some of the QDs fell out of

suspension and became part of the pellet. It is possible that the incorporation of Gd into these samples led to an unstable crystal structure and a decrease in surface ligands, and ultimately, resulted in the QDs inability to remain in solution. After this step, all samples were washed twice with a solution of 70% methanol: 30% chloroform. If the QDs are washed more than this, it can potentially remove ligands from the surface of the QDs, making them unstable in organic solvent.

3.2 Water Solubilization of QDs

To impart biological relevance, it is imperative to transfer QDs from the organic solvent in synthesis into aqueous solution. This was achieved by exchanging the native dodecanethiol ligands present after synthesis with 11-mercaptoundecanoic acid (MUA), an amphiphilic molecule that can bind to the surface of the QD and has a terminal hydrophilic carboxylate moiety. The amount of MUA added was in excess of the amount theoretically needed to ensure the highest yield of water-soluble product possible. The success of this method was assessed by centrifuging (~5,000 x g) the emulsion to separate the organic and aqueous layers. The QDs were observed to move from the organic layer on the bottom to the aqueous layer on top, which can be checked by UV light (Figure 11). When each sample was centrifuged, 3 layers typically were seen: the top aqueous layer, a middle layer in between the two phases where some QDs could be seen that weren't fully water-soluble, and the bottom organic layer. Occasionally, the bottom organic layer evaporated overnight, decreasing the visibility of an organic layer. To remove any aggregates and move samples into a buffer, all samples were dialyzed and subsequently put through a syringe filter. Samples were then stored at 4°C and observed to be stable for many months. If a sample is not stable, a pellet will form in the bottom of the centrifuge tube.

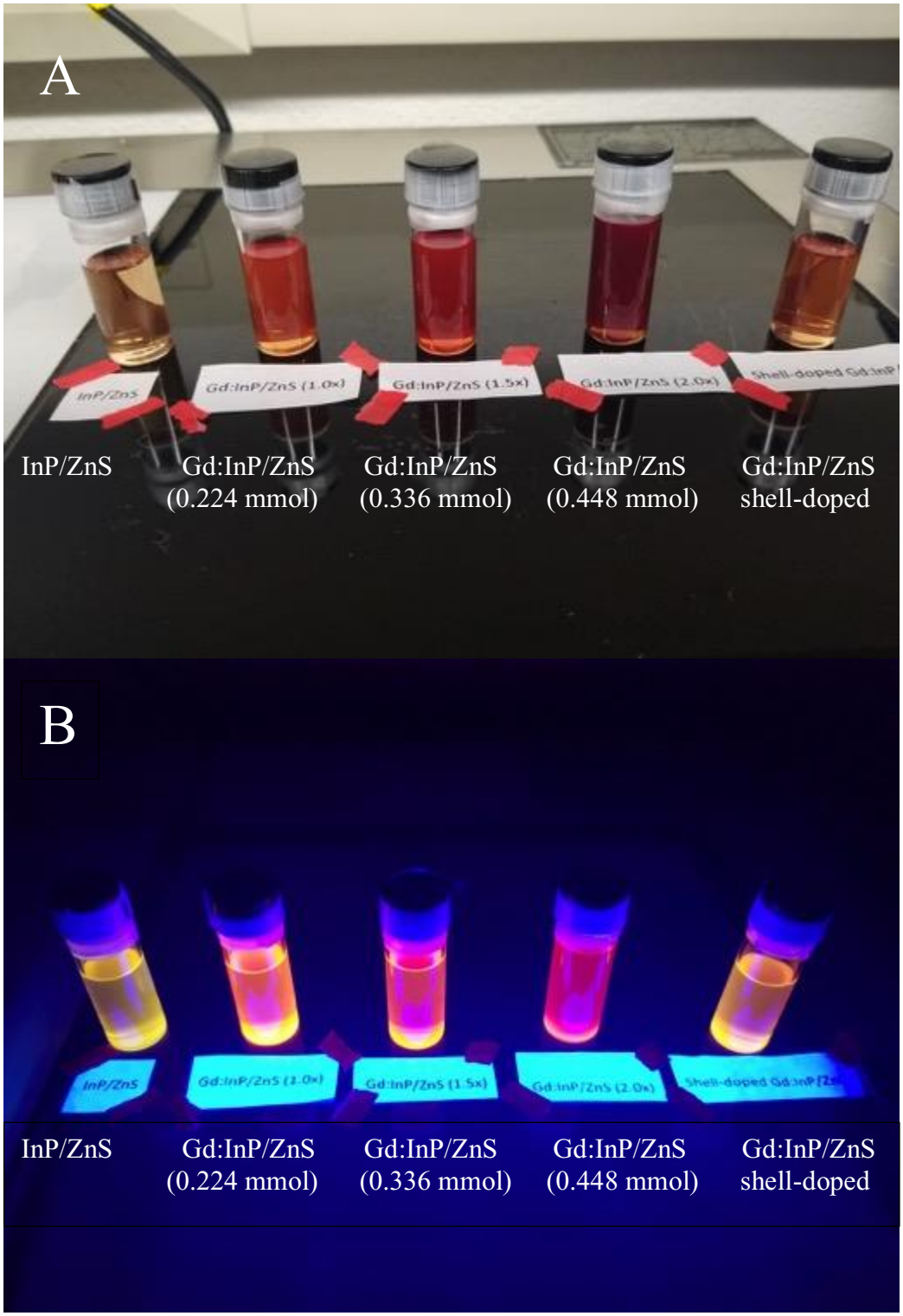

Figure 10: Synthesized QD samples under ambient and UV light. A: A diluted sample from each QD synthesis is shown as it appeared under ambient light. B: Each diluted sample is shown as it appeared to the eye under UV light.

3.3 Absorbance and Fluorescence Spectroscopy

As a starting place for characterization, absorbance and fluorescence spectra were collected for all the samples. Using the absorbance spectra, the size and concentration of QDs were determined. In order to get the data points for calculations, the maximum wavelength at the shoulder and the corresponding wavelength were taken. By calculating the particle size via calculations produced by previous studies[38], the extinction coefficient was also determined, and subsequently, the concentration. The fluorescence emission spectra showed a relative size distribution of QDs in a sample via its full-width half maximum (FWHM). This gave a relative particle size distribution as well as showed potential spectroscopic characteristics indicating QD defects[38]. Defects in the surface of the nanocrystal creates traps, or nonradiative recombination sites, causing weak fluorescence.

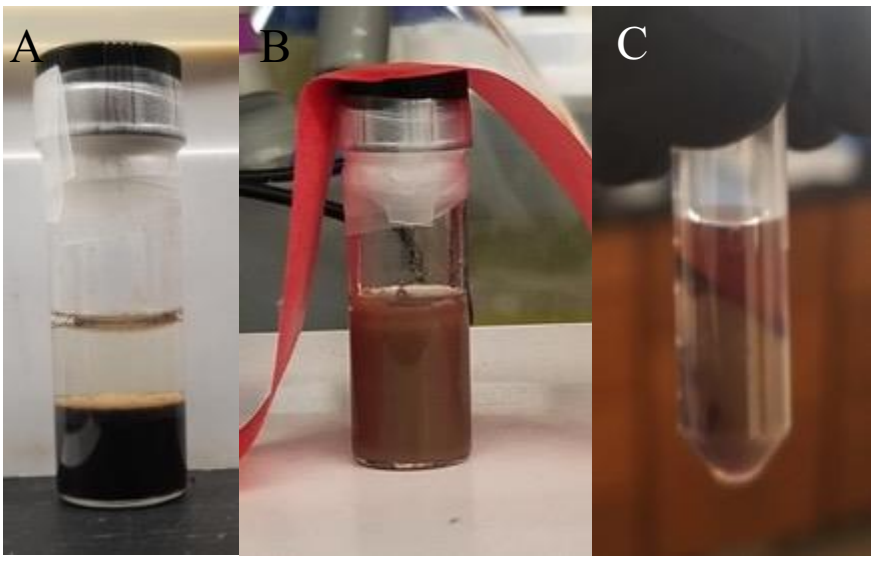

Figure 11: Stages of water solubilization. A: Before QDs were solubilized, they were on the bottom layer in the organic phase, with the TMAH-MUA mix on top. B: QDs were placed on a stir plate with a stir bar to create an emulsion between the two phases. C: After centrifugation the QDs can be seen in the top layer. The middle layer usually seen prevails in this picture, likely due to evaporation by the organic layer during solubilization.

The syntheses performed here produced QDs ranging from ~3-3.6 nm, calculated based on absorption data collected for each sample (Figure 12). The particle sizes calculated via UV-Vis spectra can be correlated with color of the QD, further confirmed through the fluorescence emission spectra (Figure 13). From largest to smallest particle size, the QD samples are Gd:InP/ZnS (0.448 mmol), InP/ZnS, Shell-doped Gd:InP/ZnS, Gd:InP/ZnS (0.336 mmol), and Gd:InP/ZnS (0.224 mmol). This same trend is followed in the fluorescence data with the largest

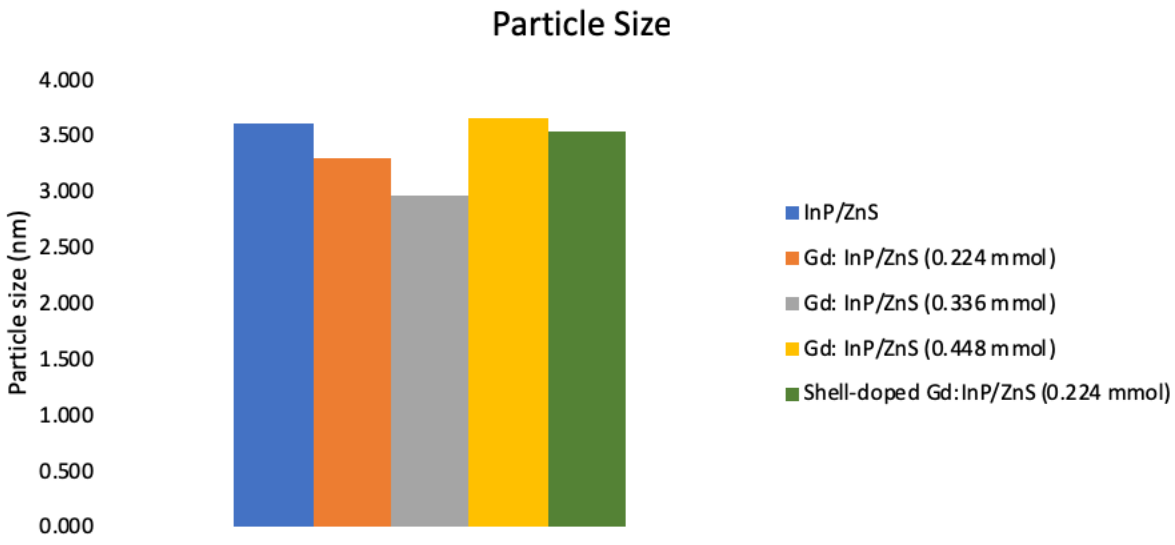

Figure 12: QD particle size. In the samples with 0.224 mmol and 0.336 mmol Gd added to the reaction, there appears to be a slight decrease in particle size. It is possible that during the synthesis water was present in the system inhibiting growth, leading to the change in size seen here[39].

QD being the most red shifted, and the smallest shifted more toward the blue. No particular trend was found in respect to concentration, though all core-doped samples had a higher concentration than both the non-doped and shell-doped, which were fairly similar. The highest concentration sample was that of Gd:InP/ZnS (0.336 mmol) that was calculated to be 56.5 μM, much higher than any of the others. Gd:InP/ZnS (0.224 mmol) and (0.336 mmol) had concentrations 13 μM and 22 μM respectively while both non-doped and shell-doped QDs came

to around 8 μM. To note, calculations for Gd-doped dots were not verified due to the complexity of the calculations, and thus by using the calculations for non-doped dots, error may have been introduced. Due to the difference in atomic radii size between In and Gd, and the assumption Gd is replacing In, the larger radii from Gd could be skewing the calculations somewhat, giving an artificially higher concentration.

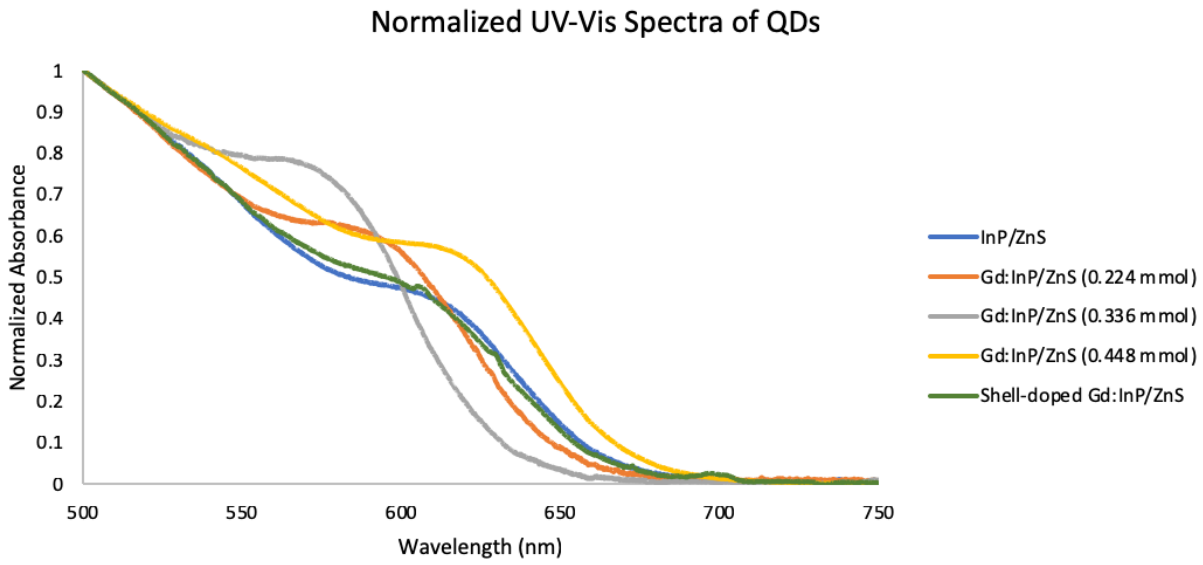

Figure 13: UV-Vis Absorption Spectra of non-doped and Gd-doped InP/ZnS QDs. UV-vis spectra of QD samples were collected, and the maximum of the shoulder was used to calculate average particle size and final concentration of the synthesized sample.

From the stock concentrations, each QD product was diluted to ~1 μM and the fluorescence spectra were obtained. These spectra were analyzed to discern the overall size distribution of QD nanoparticles (Figure 14). Addition of Gd did not seem to have an appreciable effect on size distribution. Non-doped QDs and Gd:InP/ZnS (0.0224 mmol) both had similar FWHM at around 62 nm. Gd:InP/ZnS (0.336 mmol) measured with a FWHM around 75 nm, Gd:InP/ZnS (0.448 mmol) around 68 nm, and shell-doped Gd:InP/ZnS around 71 nm. Commercially available InP/ZnS QDs with low size distributions exhibit a FWHM below 70

nm[10,40]. Thus, it does not appear that incorporation of Gd had an effect on particle size. However, this larger size distribution is potentially due to the fact that these reactions were scaled-up to produce sufficient QD products for the characterization herein. It is possible that increasing the scale of these reactions affected the reaction kinetics. Future work on this project may attempt to optimize size distribution of QD products at this scale. Additionally while observed by eye that the Gd:InP/ZnS (0.448 mmol) sample is more red-shifted than that of undoped InP/ZnS, both samples share a close lambda maximum for emitted wavelengths. The differences in these observations are likely due to the overlap in size distributions of the particles, with the majority of QDs synthesized with less Gd slightly blue-shifted.

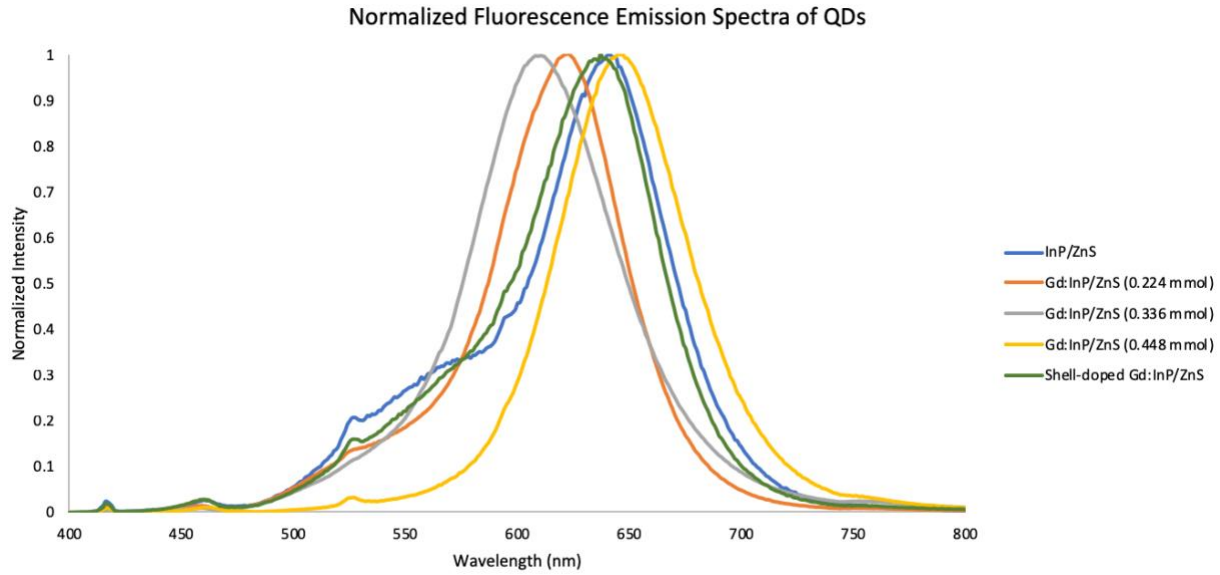

Figure 14: Fluorescence Emission Spectra of non-doped and Gd-doped InP/ZnS QDs. Fluorescence spectra of QDs show the relative size distribution of QDs in solution. As the QD size increases, the spectra become more red-shifted.

3.4 Scanning Transmission Electron Microscopy

Following synthesis, samples of different QDs were sent for Scanning Transmission Electron Microscopy (STEM) analysis at Jordon Valley Innovation Center (JVIC) (Springfield,

MO) to assess the size and shape dispersity of the nanoparticles. Non-aggregated, monodisperse particles are important for biological studies due to the unpredictability of aggregates. Non-doped InP/ZnS, Gd:InP/ZnS (0.224 mmol), and Gd:InP/ZnS (0.336 mmol) were imaged in this study (Figure 15). Non-doped QDs demonstrate some aggregation in the micrographs with clusters of 7-8 QDs closely bunched together throughout the image. It is possible, while diluting

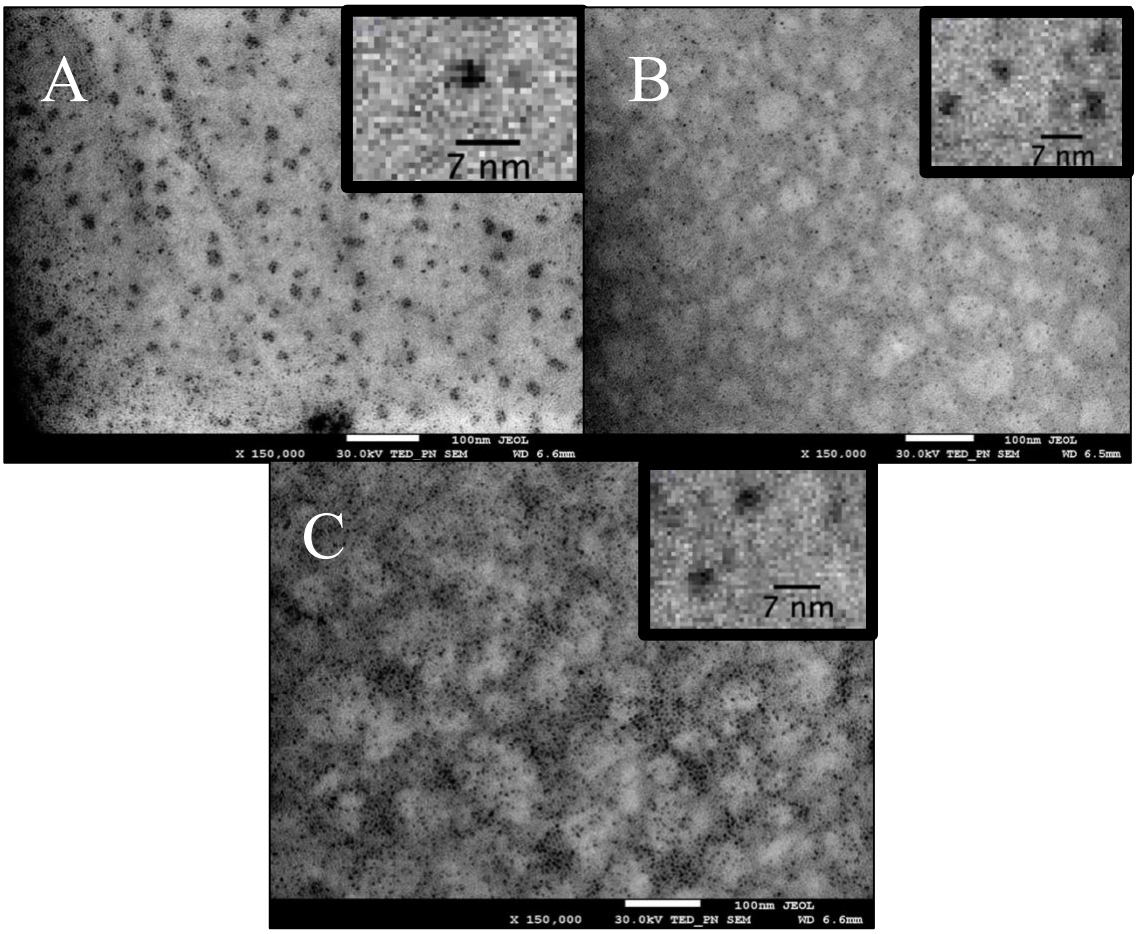

Figure 15: STEM micrographs demonstrating monodispersity of QDs. STEM images of non-doped and Gd-doped InP/ZnS QDs showing the monodispersity of (a) InP/ZnS QDs, (b) Gd:InP/ZnS (0.224 mmol), and (c) Gd:InP/ZnS (0.448 mmol) QDs. For each image, an insert shows a zoomed in area of the displayed image. A scale bar for the insert was calculated and generated based on the size of each pixel in the image.

this sample to a sufficient concentration for imaging, the sample could have become unstable. Previous observations in our lab have shown that samples are not stable at very low

concentrations. Regardless, individual QDs appeared monodisperse in size and shape. Gd-doped samples appeared clearly monodisperse and can be easily differentiated from each other, demonstrating that incorporation of Gd at the amounts used in these syntheses does not have an appreciable effect on the shape or size of the nanoparticles. Analysis of the micrographs showed the samples have a size of ~3.5 nm, which closely matched with the estimated size of the InP/ZnS QDs through calculations (Figure 12). While it would be interesting to see the STEM imaging results for Gd:InP/ZnS (0.448 mmol) and shell-doped Gd:InP/ZnS QD samples, research limitations prevented collection of this data.

3.5 Elemental Analysis via Inductively Coupled Plasma-Mass Spectrometry (ICP-MS)

In order to determine the amount of Gd incorporated into the QDs and the elemental composition of the nanoparticles, ICP-MS was performed. Three separate ICP-MS analyses were performed for each sample (Figure 16). The ratio of Zn to S is less than one for all QD samples analyzed, indicating an abundance of sulfur. However, this is likely attributed to the presence of S in the dodecanethiol ligand coating the exterior of the QD. Additionally, this analysis reveals that an increased amount of Gd in the reaction corresponded to an increase in the amount of Gd incorporated into the QD. However, the ratio of Gd/In does not increase at the same molar ratio at which it is incorporated, which is may be due to the kinetics of the reaction and presents opportunities for future work in this area. Further, results indicated a discrepancy in the ratio of Gd and In to P. The expected ratio would be 1:1; however for Gd:InP/ZnS (0.224 mmol) the ratio was 1.56. This observation could be an indication of oxidation, with a decrease in P being seen as a result.

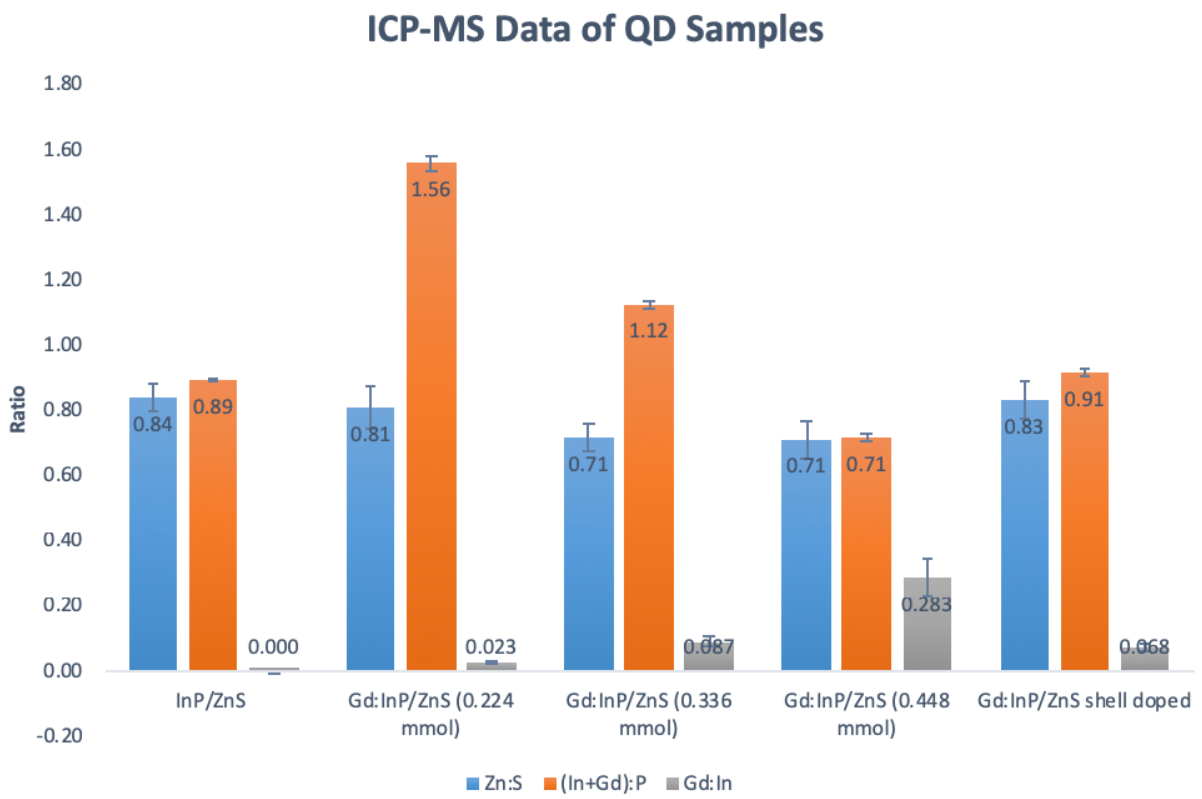

Figure 16: Elemental analysis of QD samples analyzed via ICP-MS. Using ICP, the molar ratios of Zn:S, (In+Gd):P, and Gd:In were found. This was used to determine the success of the synthesis as well as the amount of Gd incorporated into the QDs.

3.6 MRI Contrasting Capabilities

In order to investigate MRI capabilities of the QDs, water-solubilized QD samples were sent to Dr. Jens Rosenberg at the National High Magnetic Field Lab (Tallahassee, Florida). Three concentrations (1μM, 500 nM, and 100 nM) of QD solution were analyzed. While nanomolar concentrations are relevant in *in vivo* application of QDs, a concentration of 1 μM was also used since it is most likely to have visible contrast[41,42]. For each sample, both T_1 and T_2 relaxation data was gathered.

For the samples sent for characterization, the image maps generated for T_1 and T_2 relaxation were compared to a conventional contrasting agent used in clinical MRI, gadodiamide (Omniscan™). When the analysis was performed, the data for the top and bottom rows of Figure

17 were taken separately from each other. Samples in the top row (dissolved in a PBS) appeared brighter because the software scaled the image to the brightest voxel. In the top row, the brightest voxel was from water, making the samples appear bright, though their relaxation time was not actually considerably short (Figure 17, Figure 18). For the bottom row of samples and the PBS control, however, samples were scaled to gadodiamide. In T_1 contrast if the relaxation time is short, one would expect a bright contrast. The samples in the bottom row of Figure 17 appear

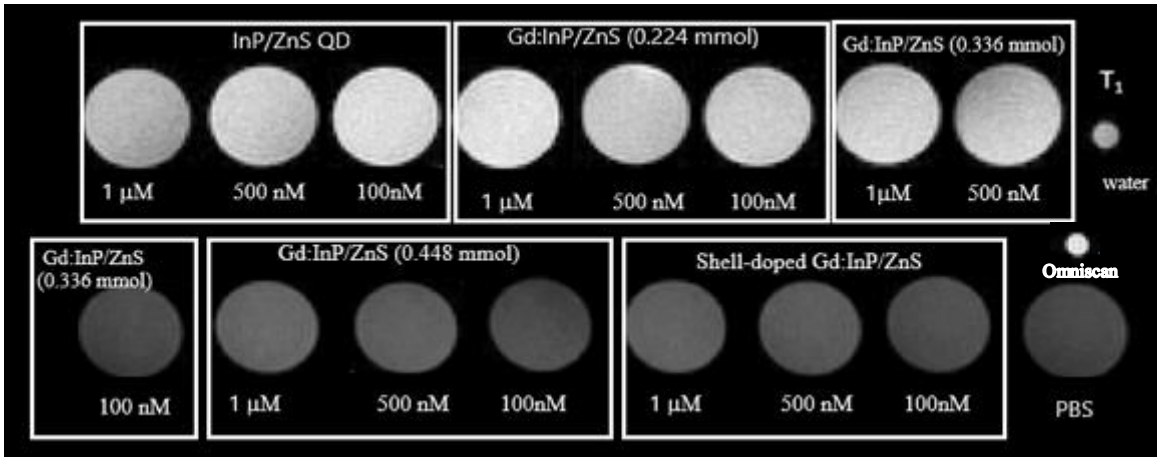

Figure 17: Mapped T_1 relaxation times for QD samples. Samples were measured in an NMR with a 21.1 Tesla magnet fitted with an imaging probe. Pixels in the top row were scaled to the brightest pixel of the water sample, while pixels in the bottom row were scaled to the brightest pixel of the Omniscan sample.

darker than the top row because the samples on the bottom row were scaled to gadodiamide (with a very low T_1 of 15.9 ms). When comparing both the images and relaxation times, a modest increase in brightness in the samples can be seen, especially when compared with the PBS control. Additionally there is a modest decrease in relaxation time for the more concentrated samples of Gd:InP/ZnS (0.448 mmol) and shell-doped Gd:InP/ZnS QDs. While a relatively small amount of Gd was added to the shell-doped sample (0.224 mmol), the relaxation displayed by the shell-doped sample is much more comparable to a higher doped sample. This is likely a

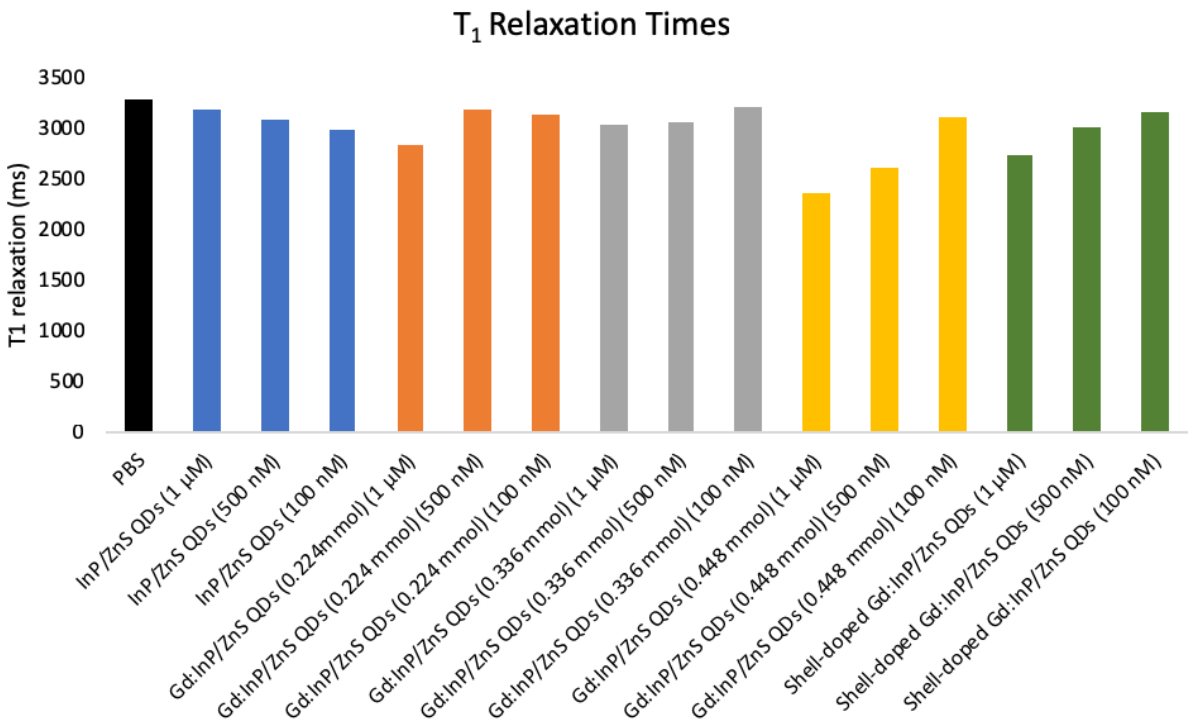

Figure 18: Average T_1 relaxation times for QDs. While modest, Gd:InP/ZnS (0.448 mmol) and shell-doped Gd:InP/ZnS QDs at higher concentrations show a decrease in T_1 time compared to PBS.

result of the Gd being closer to the surface of the QD, and as a result, causing a more noticeable relaxation in the nearby water molecules. However, the relaxation times for these QD samples were around 2200 ms and above; since promising contrast agents are typically below 1000 ms, T_1 contrast does not appear to be a suitable modality for these QDs[43].

Gd-doped QDs show a more prominent potential as a T_2 contrast agent. All images in Figure 19 were scaled to gadodiamide, which has a T_2 time too short for it to be visually noticeable. Both Gd:InP/ZnS (0.448 mmol) and shell-doped QD images are visibly darker than that of the PBS control or undoped QD images.. Additionally, these samples demonstrate a clear reduction in relaxation times compared to the PBS control (Figure 20). T_2 relaxation for the PBS control was around 400 ms, while samples from both the Gd:InP/ZnS (0.448 mmol) and shell-

doped Gd:InP/ZnS samples had relaxation times around 100-140 ms and 180-190 ms respectively in the 1 μM and 500 nM concentrations. The typical contrast agent has a T_2

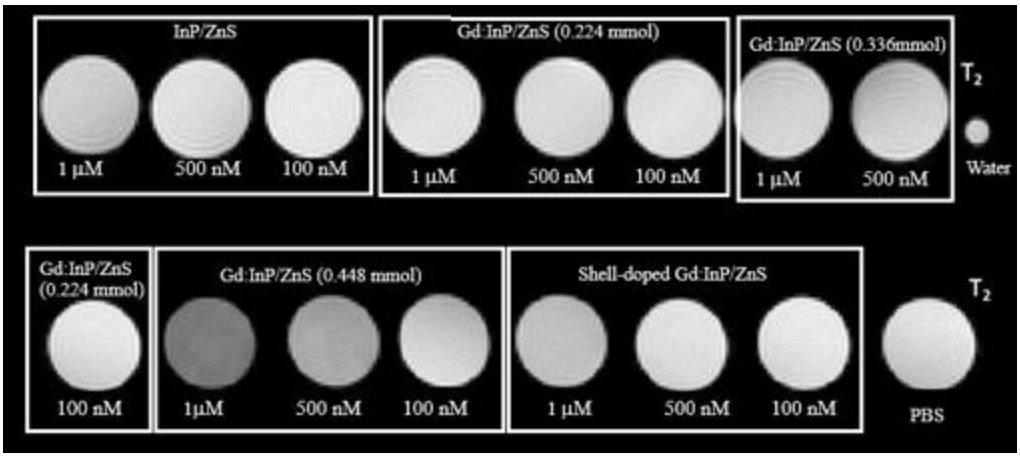

Figure 19: Mapped T_2 relaxation times for QD samples. Samples were measured in an NMR with a 21.1 Tesla magnet fitted with an imaging probe and scaled to Omniscan. The Omniscan T_2 relaxation was much shorter than the samples, which caused it to be too dark to appear.

relaxation of 100 ms or lower[43]. As with T_1, the shell-doped sample shows improved contrast, similar to Gd:InP/ZnS (0.448 mmol). The Gd in this sample, however, was closer to the surface of the QD, thus closer to the aqueous solvent and likely allowing a larger effect on water molecules. Comparatively, the contrast seen in the QD samples was modest compared with gadodiamide, which has a relaxation around 9.3 ms.

3.7 MTT Cell Viability Assay

In order for Gd-doped QDs to be a feasible diagnostic tool, the cytotoxicity must be examined. Here, toxicity was studied using an MTT assay, which uses cellular respiration as a baseline for viability. A wide range of QD concentrations were used to assess cellular viability. QD concentrations of 100 nM- 500 nM were chosen to assess the viability in the concentration range that contrast data is often acquired[41]. Additionally, lower concentrations (250 pM- 1 nM)

were chosen to assess viability in the concentration range that is typically used for cellular labeling[41].

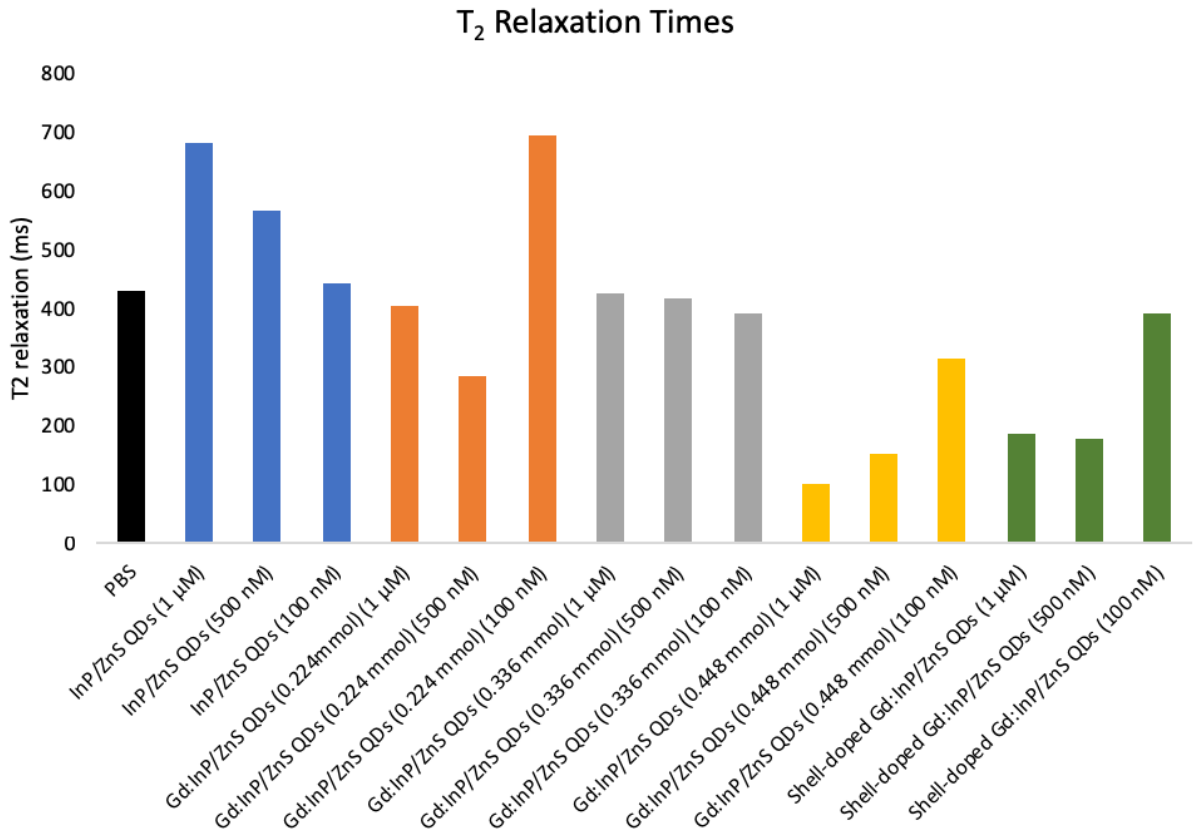

Figure 20: Average T_2 relaxation times for QDs. For both Gd:InP/ZnS (0.448 mmol) and shell-doped Gd:InP/ZnS QDs, there was a noticeable decrease in T_2 relaxation when compared against the control, presenting potential for use as an MRI contrasting agent.

A decrease in viability was observed in cells treated with higher concentration of the QD samples, especially for shell-doped Gd:InP/ZnS (Figure 21). For the cells treated with 250 pM – 1nM QDs, the cell viability remains above 80%. However, a trend can be seen that with increased Gd content, there is a decrease in cell viability. For higher concentrations (100 nM-500 nM), cell viability decreased in both non-doped and shell-doped samples. In the case of the non-doped samples, it is possible that at this concentration particles begin to aggregate onto the cells, resulting in toxicity. STEM micrographs indicate that this sample was more prone to

aggregation (Figure 3.7). For shell-doped QDs, Gd was closer to the surface of the QD; therefore, Gd is more likely to be released into the surrounding medium. At 250 nM and 500 nM, QDs with the highest Gd content (0.448 mmol) cause a decrease in cell viability below 80 %. While higher concentrations of QDs show cytotoxicity, these concentrations are not typically used in cellular labeling applications[41]. QD concentrations usually used for cell targeting show little effect on cell viability.

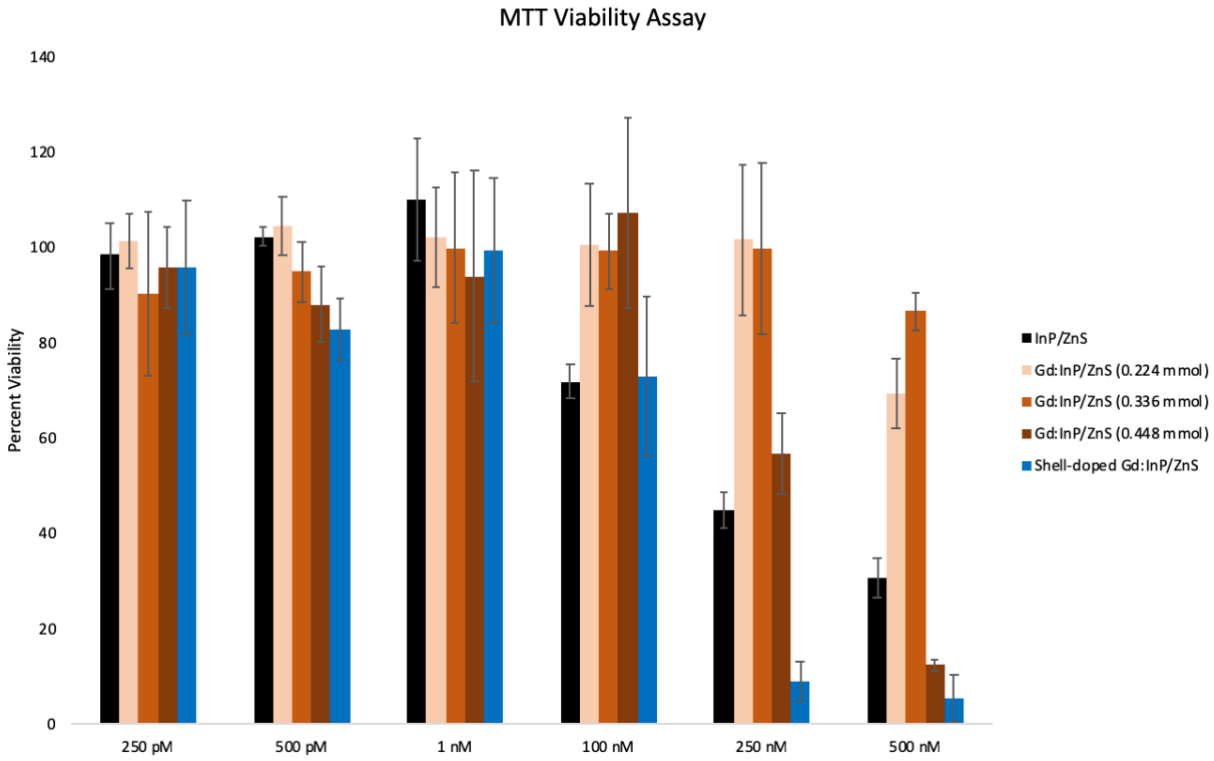

Figure 21: MTT Viability Assay for non-doped and Gd-doped InP/ZnS QDs. For most samples cellular viability does not decline below 80 % until 100 nM and above. However, for labeling, cells are usually not treated with concentrations over 100 nM QDs.

3.9 Conclusions and Future Work

This work represents a preliminary study of newly-synthesized Gd-doped QDs and their utility as an MRI contrast agent. Through absorbance data, particle size and concentration were calculated for each sample. The particle size was then compared to the lambda max of each

fluorescence spectrum. Furthermore, the fluorescence spectra FWHM were analyzed for the size distribution of the nanoparticles and potential contamination by water during synthesis. Particle size via STEM data was correlated to particle size via absorbance calculations and found to be in relative agreement (Figure 12). ICP-MS data demonstrated that the ratio of (Gd+In):P was higher than expected for Gd:InP/ZnS (0.224 mmol) and Gd:InP/ZnS (0.336 nmol) suggesting that oxygen may have been incorporated into the crystal lattice in place of P (Figure 16). Both of these samples have a smaller average size than the rest of the samples which is also indicative of oxidation (Figure 12). Assessing the samples for MRI contrast showed moderate imaging capabilities of Gd:InP/ZnS (0.448 mmol) and shell-doped QDs. While the contrast for T_1 was minimal, T_2 presented much better contrast for these samples. When assessing the toxicity of the QD samples, Gd-doped QDs do not appear to have a negative impact on cell viability within concentrations used for normal cellular labeling.

Future work could investigate using Manganese^{2+} as the shell-doping agent, due to its biocompatibility and paramagnetism. Additionally, samples could be PEGylated to assess the MRI capabilities, since it is expected that the highly hydrophilic nature of PEG may bring water molecules closer to the QD surface, and thus paramagnetic ions. As seen in the results, it is possible the kinetics of the original synthesis reaction were affected when the synthesis was scaled up, which could also be further optimized. Additionally, there is potential that more Gd could be incorporated into the crystal structure. More syntheses could be performed with increased mmol amounts of Gd until potentially QDs are unable to be formed. This work provides many potential avenues for further development and optimization for an MRI-active QD.

REFERENCES

(1) Xu, G.; Zeng, S.; Zhang, B.; Swihart, M.; Yong, K.; Prasad, P. *Chem. Rev.,* 2016, *116*, 122234.

(2) Wang, L.; Chen, L. *Nanomedicine,* **2011**, *7*, 385

(3) Reiss, P.; Protiere; Li, L. *Small,* **2009**, *5*, 154.

(4) Michalet, X.; Pinaud, F.; Bentolila, L.; Doose, S.; Li, J.; Sundaresan, G.; Wu, A.; Gambhir, S.; Weiss, S. (2008). *Science*, **2008**, *307*, 538.

(5) Talapin, D.V.; Lee. J.; Kovalenko, M.V.; Shevchenko, E.V. *Chem. Rev.*, **2010**, *110*, 389.

(6) Collier, C.P.; Vossmeyer, T.; Heath, J.R. *Annu. Rev. Phys. Chem.,* **1998**, *49*, 371.

(7) Ashoori, R.C. *Nature*, **1996**, *380*, 559.

(8) Bawendi, M. *Annu. Rev. Phys. Chem.,***1990**, *41*, 477.

(9) Yoffe, A.D. *Adv. Phys.,* **2001**, *50*, 1.

(10) Millipore Sigma Home Page. https://www.sigmaaldrich.com (accessed February 22, 2019).

(11) Olympus - Life Science Solutions Home Page. https://www.olympus-lifescience.com (accessed February 22, 2019).

(12) Toufanian, R.; Piryatinski, A.; Mahler, A.; Iyer, R.; Hollingsworth, J.; Dennis, A. *Front. Chem.*, **2018**, *6*, 1.

(13) Murphy, C.J.; Coffer, J.L. *Appl. Spectrosc.*, **2002**, *56*, 1.

(14) Mushonga, P.; Onani, M.O.; Madiehe, A.M.; Meyer, M. *J. Nanomater.*, **2012**, *2012*, 1.

(15) Pong, B.; Trout, B.; Lee, J. *Langmuir,* **2008**, *24*, 5270.

(16) Cossairt, B.M. *Chem. Mater.,* **2016**, *28*, 7181.

(17) Tessier, M.D.; De Nolf, K.; Dupont, D.; Sinnaeve, D.; De Roo, J.; Hens, Z. *J. Am. Chem. Soc.,* **2016**, *138*, 5923.

(18) Tamang, S.; Lincheneau, C.; Hermans, Y.; Jeong, S.; Reiss, P. *Chem. Mater.,* **2016***, 28*, 2491.

(19) Xu, S.; Ziegler, J.; Nann, T. *J. Mater. Chem.*, **2008**, *18*, 2653

(20) Song, W.; Lee, H.; Lee, J. C.; Jang, D. S.; Choi, Y.; Choi, M.; Yang, H. *J. Nano. Res.,* **2013**, *15*.

(21) Tamang, S.; Beaune, G.; Texier, I.; Reiss, P. *ACS Nano,* **2011**, *5*, 9392.

(22) Pong, B.; Trout, B.; Lee, J. *Langmuir,* **2008**, *24*, 5270.

(23) Mocatta, D.; Cohen, G.; Schattner, J.; Millo, O.; Rabani, E.; Banin, U. *Science,* **2011**, *332*, 77.

(24) Makker, M.; Viswanatha, R. *RSC Adv.* **2018**, *8*, 22103.

(25) Pradham, N.; Goorskey, D.; Thessing, J.; Peng, X. *J. Am. Chem. Soc.,* **2005**, *127*, 17586.

(26) Bera, D.; Qian, L.; Tseng, T.; Holloway, P. *Materials,* **2010**, *3*, 2260.

(27) Rohrer, M.; Bauer, H.; Mintorovitch, J.; Requardt, M.; Weinmann, H. *Invest. Rad.*, **2005**, *40*, 715.

(28) Van Geuns, R.; Wielopolski, P.; de Bruin, H.; Rensing, B.; van Ooijen, P.; Hulshoff, M.; Oudkerk, M.; de Feyter, P. *Progress in Cardiovascular Diseases*, **1999**, *42*, 149.

(29) Levitt, M. H. *Spin Dynamics: Basics of nuclear magnetic resonance*. Wiley: New York, NY, 2015; pp 315-336.

(30) Preston, D.C. Magnetic Resonance Imaging (MRI) of the Brain and Spine: Basics. http://casemed.case.edu (accessed March 6, 2019).

(31) Barber, T.; Klein, J.; Mackay, C.; Hu., M. *Neuroimage: Clinical*, **2017**, *15*, 215.

(32) Godau, J.; Hussi, A.; Lolekha, P.; Stoessl, A.J.; Seppi, K. *Mov. Disord.*, **2012**, *27*, 634.

(33) Chiti, F.; Dobson, C.M. *Annu. Rev. Biochem.,* **2006**, *75*, 333.

(34) Cree, I.A. *Cancer Cell Culture: Methods and Protocols*. Humana Press: Totowa, 2016; pp 237-245.

(35) Morgan, D.M.L. *Methods in Molecular Biology*™. Humana Press: Totowa, 1998; pp 179-184.

(36) Ellis, M.A.; Grandinetti, G.; Fichter, K. M. *J. Vis. Exp.*, **2016**, e53684.

(37) Xie, R.; Li, Z.; Peng, X. *J. Amer. Chem. Soc.*, **2009**, *131*, 15457.

(38) Yang, X.; Zhao, D.; Leck, K.; Tan, S.; Tang, Y.; Zhao, J.; Demir, J.; Sun, X. *Adv. Mater.,* **2012**, *24*.

(39) Ramasamy, P.; Kim, B.; Lee, M.; Lee, J. *Nanoscale*, **2016**, *8*, 17159.

(40) Creative Diagnostics Home Page. https://www.cd-bioparticles.com (accessed May 25, 2019).

(41) Brunetti,V.; Chibli, H.; Fiammengo, R.; Galeone, A.; Malvindi, M.; Vecchio, G.; Cingolani, R.; Nadeau, J.; Pompa, P. *Nanoscale,* **2013**, *5*, 307.

(42) Gao, X.; Cui, Y.; Levenson, R.; Chung, L.; Nie, S. *Nat. Biotechnol.,* **2004**, *22*, 969.

(43) Bottomley, P.; Hardy, C.; Argersinger, R.; Allen-Moore, G. *Med. Phys.*, **1987**, *14*.